AD-783 717

# DEVELOPMENT OF ELECTRIC: FIELD SENSORS

William C. Taylor, et al

Stanford Research Institute

Prepared for:

Defense Nuclear Agency

26 February 1974

DESTROY THIS REPORT WHEN IT IS NO LONGER NEEDED.

DO NOT RETURN TO SENDER.

Field Command Printing Division

UNCLASSIFIED

SECURITY CLASSIFICATION OF THIS PAGE (When Data Entered)

## REPORT DOCUMENTATION PAGE

READ INSTRUCTIONS BEFORE COMPLETING FORM

| | |
|---|---|
| 1. REPORT NUMBER<br>DNA 3259F | 2. GOVT ACCESSION NO. |
| 3. RECIPIENT'S CATALOG NUMBER<br>AD-783 717 | |
| 4. TITLE (and Subtitle)<br>DEVELOPMENT OF ELECTRIC-FIELD SENSORS | 5. TYPE OF REPORT & PERIOD COVERED<br>Final Report for Period<br>1 Jun 72 — 15 Sep 73 |
| | 6. PERFORMING ORG. REPORT NUMBER<br>SRI Project 1973 |
| 7. AUTHOR(s)<br>William C. Taylor<br>Arthur L. Whitson<br>Duane C. Gates | 8. CONTRACT OR GRANT NUMBER(s)<br>DNA 001-72-C-0102 |
| 9. PERFORMING ORGANIZATION NAME AND ADDRESS<br>Stanford Research Institute<br>333 Ravenswood Avenue<br>Menlo Park, California 94025 | 10. PROGRAM ELEMENT, PROJECT, TASK AREA & WORK UNIT NUMBERS<br>NWET Subtask<br>J11AAXE430-02/03 |
| 11. CONTROLLING OFFICE NAME AND ADDRESS<br>Director<br>Defense Nuclear Agency<br>Washington, D.C. 20305 | 12. REPORT DATE<br>26 February 1974 |
| | 13. NUMBER OF PAGES<br>77 |
| 14. MONITORING AGENCY NAME & ADDRESS(if different from Controlling Office) | 15. SECURITY CLASS. (of this report)<br>UNCLASSIFIED |
| | 15a. DECLASSIFICATION/DOWNGRADING SCHEDULE |

16. DISTRIBUTION STATEMENT (of this Report)

Approved for public release; distribution unlimited.

17. DISTRIBUTION STATEMENT (of the abstract entered in Block 20, if different from Report)

18. SUPPLEMENTARY NOTES



Details of illustrations in this document may be better studied on microfiche.

19. KEY WORDS (Continue on reverse side if necessary and identify by block number)

| | |
|---|---|
| Internal Electromagnetic Pulse (IEMP) | Potential Measurements |
| IEMP Sensor | Radiation Effects |
| EMP Sensor | Aurora Facility |
| Electric-field Measurements | Transmission-line Coupling |

20. ABSTRACT (Continue on reverse side if necessary and identify by block number)

The purpose of this program was to obtain parametric data and develop criteria needed in the design of wire-mesh-type electric-potential sensors for arbitrary EMP and IEMP environments. Tests were performed with various grid materials, thicknesses, and configurations in selected environments provided by the Febetron 706, Febetron 705, and Aurora flash gamma-ray machines, with varied environmental parameters such as air pressure and cavity material. It is shown that this technique can be used successfully when an essentially open-circuit voltage measurement

DD FORM 1 JAN 73 1473 EDITION OF 1 NOV 65 IS OBSOLETE

UNCLASSIFIED

SECURITY CLASSIFICATION OF THIS PAGE (When Data Entered)

20. ABSTRACT (Continued)

is made, provided that care is taken to prevent large amounts of charge from being deposited on or scattered from the grid, which causes it to depart from the space-charge potential it is intended to measure. The various sources of these charges are described, and methods of minimizing the problem have been demonstrated. Furthermore, a method is illustrated that allows discrimination between the desired space-charge potential and the error-producing charge-deposition potential.

The tests in DNA's Aurora facility confirmed the viability of the sensors developed for use in that facility. Also described are measurements of potential and of fields using low-impedance techniques that are seen to present difficulties in interpretation. Some measurements of coupling to transmission lines in the Aurora facility test cell were performed and are reported. Measurements of the electric field in the open test cell, using two parallel grids, are also described. A one-dimensional analysis was performed, providing estimates of the maximum potentials reached and of the time in the pulse when the ionized-air effects tend to neutralize the fields, causing them to reach an early maximum.

# PREFACE

The authors gratefully acknowledge the following:

- Douglas Webb, who either performed or assisted with all the measurements reported here.
- G. R. Hilbers and W. C. Wadsworth for designing the amplifiers for the Aurora tests.
- Capt. Robert Antinone and Mr. Al Hoffland of Air Force Weapons Laboratory for assistance in the Febetron 705 measurements.
- Stewart Graybill and the remainder of the Aurora Staff for assistance in the Aurora measurements.
- John Tompkins, John Rosado, and Ralph Genuario of Harry Diamond Laboratory for stimulating discussions and for providing some equipment for the Aurora tests.

TABLE OF CONTENTS





Preceding page blank

## LIST OF ILLUSTRATIONS

TABLE

# I INTRODUCTION

For several years it has been recognized that there is a need to corroborate with measurements the predicted high electric fields and potentials produced in the deposition region of a nuclear detonation in the atmosphere. The deposition region is the region where significant photon, neutron, and/or electron fluxes exist, causing certain complications in instrumentation for such measurements. A recent description of the very complex space- and time-dependence of the fields and environments is given by Schlegel et al.[1*] Outside this deposition region, only the radiated electromagnetic pulse (EMP) is of interest. In the deposition region, in addition to the free-field phenomena produced in the air away from boundaries (other than the air/earth surface), there is also the phenomenon of IEMP (internal EMP). IEMP consists of fields and potentials produced when photons scatter Compton and photoelectrons out of walls of metal enclosures. The presence of the time-varying negative space charge produces the time-dependent field. In both EMP and IEMP, a measurement is complicated by (1) the direct interaction of a sensor with the particle fluxes, and (2) the enveloping low-energy ("conduction") plasma resulting from ionization of the air by the Compton collisions and by subsequent collisions involving electrons of successively lower energy.

Electric-field measurements were made initially in a free-field environment with a relatively low radiation level.[2] IEMP measurements were made much later in an enclosure exposed to an underground nuclear

---

*References are listed at the end of the report.

burst.[3] These measurements suggested that errors from the loss or capture of electrons by direct interaction of the sensor with photons and electrons may be significant. It was also suspected that plasma-sheath effects could influence the measurement.

These possible sources of error in the measurements prompted a series of two experimental programs of laboratory measurements to study the radiation effects in general and to provide parametric data oriented toward design of sensors to operate in a wide range of environments. In the first of these programs,[4] measurements were made in the X-ray field produced by a Febetron 706 flash X-ray machine and in a 1-MeV electron accelerator. This study confirmed the feasibility of using fine-wire meshes for IEMP potential measurements in certain environments.

The second program is the subject of this report. The objective of this program was to develop criteria and parametric data needed in the design of electric-field and electric-potential sensors. The results of the study were then used to develop a sensor for use in the environment of DNA's Aurora facility near Washington, D.C.

## II OVERVIEW AND SUMMARY

### A. General

The emphasis of this program has been on gathering experimental data on the performance of electric-field sensors in a radiation environment. Limited analysis has been performed to delineate the various effects that combine to produce both the desired signal and the spurious ones.

The measurements were made in the photon beams of three different flash X-ray machines. Some of the important characteristics of these beams are shown in Table 1. With the relatively narrow Febetron beams, we used lead between the machine and the experiment to further collimate the beams. On the other hand, in the widespread Aurora beam, lead was used to shield the electronic equipment and cables from TREE effects (Transient Radiation Effects on Electronics).

### B. Open-Circuit Measurements with Wire-Mesh Grids

The vast majority of the tests were made with fine-wire meshes placed in nominally equipotential planes, as depicted in Figure 1. Figure 2 is a photograph of the equipment used in room-pressure tests, and Figure 3 shows the two chambers used for low-pressure tests. Electrons forward-scattered from the emissions plate and backscattered from the end plate generate the space-charge fields.

The most straightforward measurement to interpret is the open-circuit voltage of the grid. In the absence of spurious charge deposition on the grid, the open-circuit voltage of the grid will be the potential generated by the scattered Compton and photoelectrons in the plane of the grid. However, there are several processes by which

Table 1

COMPARISON OF PHOTON OUTPUTS

| | Febetron 706 | Febetron 705 | Aurora |
|---|---|---|---|
| Peak dose rate in region of grids (rad/s) | 1 to 2 $\times 10^{9}$ | 0.5 to 1 $\times 10^{10}$ | 4 to 8 $\times 10^{10}$ |
| Pulsewidth at half max (ns) | 2 | 22 | 125 |
| Maximum charging voltage | 600 kV | 2 MV | 11 MV |

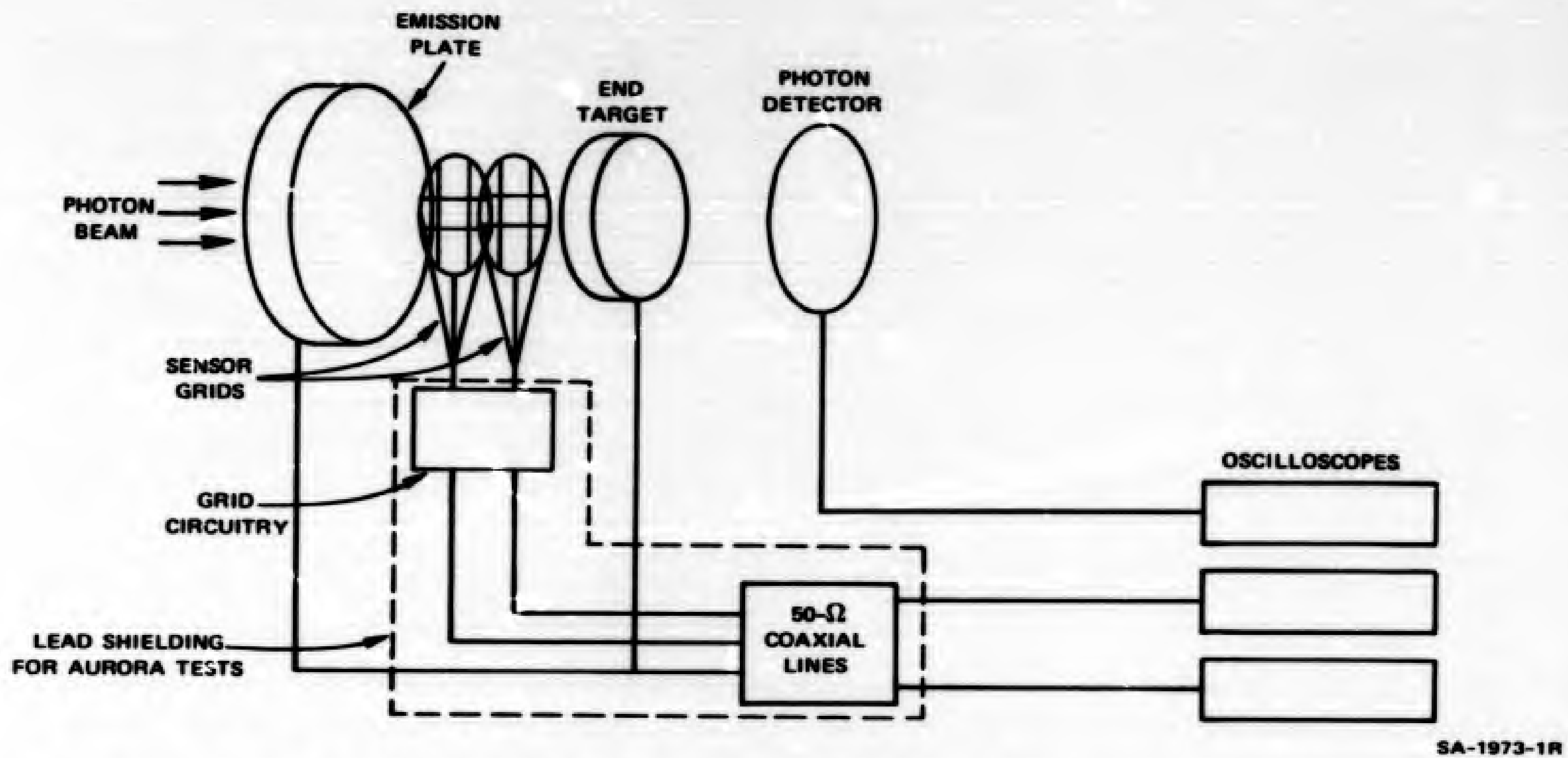


FIGURE 1 OPEN-SCHEMATIC ILLUSTRATION OF SENSOR AND CAVITY ARRANGEMENT FOR PARAMETER STUDY

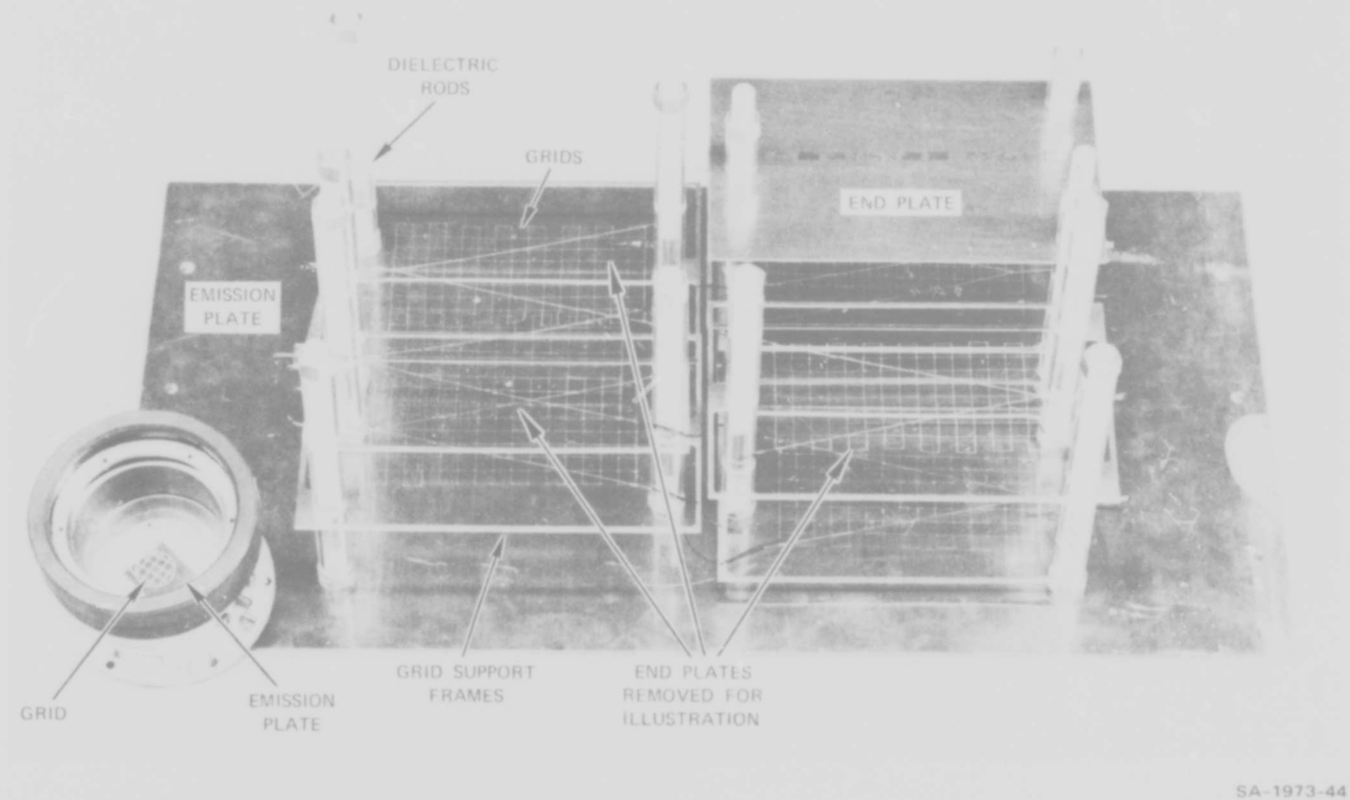


FIGURE 2 EMISSION-PLATE/GRID ASSEMBLIES FOR FEBETRON (lower left) AND FOR AURORA TESTS AT ROOM PRESSURE

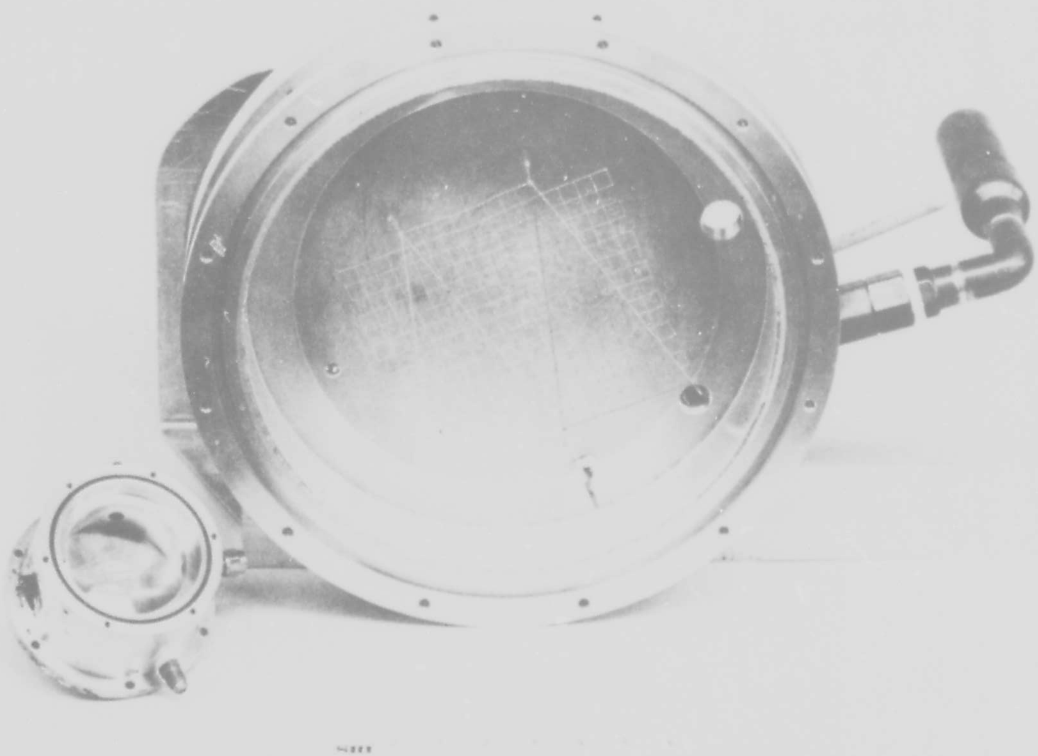

SA-1973-45

FIGURE 3 INTERIOR AND GRIDS OF VACUUM CHAMBERS USED FOR TESTING IN FEBETRONS (lower left) AND AURORA a grid can exchange charge with its environment, resulting in an unwanted deviation of the grid potential from the local (unperturbed) generated potential. It was found that the two most important of these processes are (1) the absorption by the grid wires of some of the source electrons, and (2) the scattering of electrons from the grid wires, principally by photoelectric and Compton collisions of the incident photons inside the grid wires. It was found that there could be a very large charge imbalance produced by these two processes, especially in the soft photon spectra of the two Febetrons. The polarity and magnitude of this imbalance will depend on the atomic number of the grid and of the materials constituting its environment.

Thus it is seen that in work with low-energy beams it is particularly important to (1) minimize the volume of grid material, and (2) use grids with an atomic number that effects a near balance between these two competing processes. Considerable data was taken with varied emission-plate and end-target materials and with varied air pressure, and these data are given here to guide the experiment designer in minimizing this unwanted effect. Then, for cases in which a good balance is not achieved, a method is given for discriminating the desired potential from the imbalance signal, provided that the product of grid capacitance, C, and its load resistance, R, is much greater than the duration of the desired potential pulse. This inequality is the condition for an essentially open-circuit measurement. Thus, a viable technique for measuring electric potentials is described and demonstrated for a wide variety of machine environments. Additionally, measurements of the electric <u>field</u> strength were performed using two parallel grids of relatively small separation and recording the difference in the potential for that separation. The chief disadvantage of the open-circuit measurement is that active electronics must be used to achieve a high enough RC product in most cases, compounding the photon shielding problem especially in Aurora. The grids were also used successfully to monitor potential in the Febetron 706 electron beam.

## C. Other Techniques

Measurements were made in all three machines with various sensors other than wire-mesh grids and with low-impedance loads on the sensors. Generally, these measurements were made for the following purposes: (1) to relate the open-circuit grid techniques to techniques used by other experimenters, (2) to determine if a viable low-impedance technique without active electronics could be developed that is more feasible to implement in the radiation environment then the high-impedance measurement, or (3) to attempt improvements over the simple wire-mesh configuration of the grid with respect to capacitance and radiation interaction.

These measurements include the use of short wires (monopoles) parallel to the Compton currents, terminated on only one end, and longer wires terminated at both ends, using various impedances at the terminations. Although these sensors give qualitatively understandable results, they do not give quantitative measurements as clear as those yielded by the other techniques in our present state of understanding. Also, the use of grids with low-impedance loads gives data that we have not satisfactorily interpreted.

## D. "Free-Field" Measurements

Thus far, the measurements discussed were made in cavities small compared with range, $R_e$, of the source electrons in air. For large cavity dimensions (and sufficient air pressure) the electrons forward-scattered out of the emission plate are absorbed by the air in a layer of thickness $R_e$ as shown in Figure 4. Beyond this layer the source

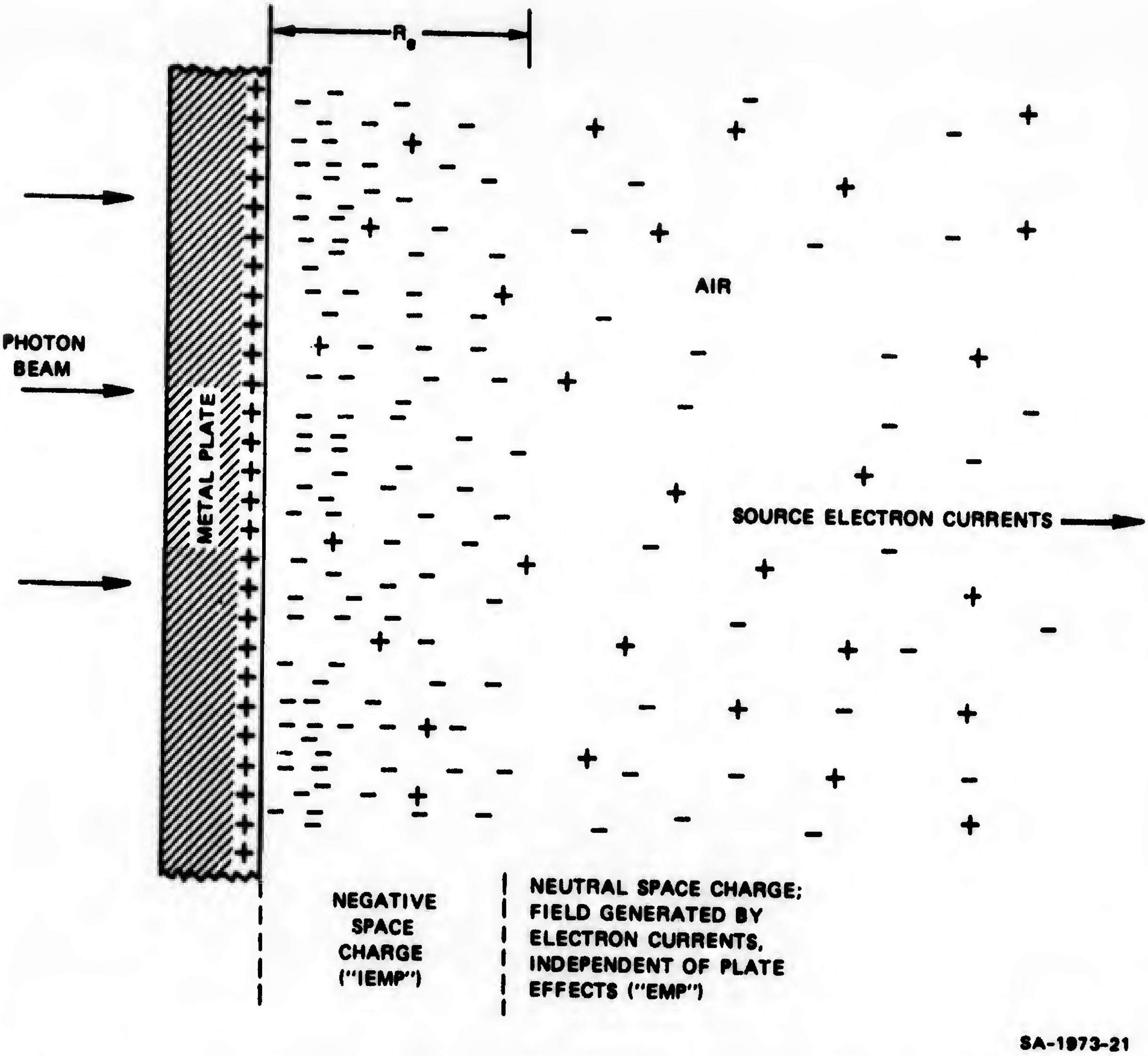


FIGURE 4 SPACE-CHARGE DISTRIBUTION DEPICTED WITHIN AND BEYOND ONE ELECTRON RANGE OF METAL PLATE, SHOWING TRANSITION FROM NOMINAL IEMP REGION TO EMP REGION

electrons will have been generated by photon collisions with the air molecules exclusively instead of collisions in the metal wall. Assuming that the photon beam is negligibly attenuated over the distance of interest, there will be charge neutrality beyond the "shadow" layer because positive ions are created by subsequent photon collisions through volume. The electron currents constitute the source of this "free" field, which is analogous to EMP rather than IEMP, since the latter is generally considered to be space-charge-generated. Usually cavity dimensions for IEMP work are much less than $R_e$ even at room pressure.

Measurements of potential and field were made in the edge of the free-field region in Aurora at two different locations, using the open-circuit-voltage measurement. One measurement gave fair agreement with the predicted range of 17 to 60 kV/m. Both measurements had time histories that were quite different from the expected ones.

## E. Conclusions

Briefly, at this juncture, the status of electric-field and -potential sensors can be stated as follows. First, the objectives of this program were achieved--i.e., the basic criteria and parametric data for design of a particular type of sensor have been produced, and specific sensor/instrumentation systems have been successfully demonstrated during the course of the testing for use in three different simulator environments, including Aurora. As for EMP (deposition region) versus IEMP measurements, the IEMP potential and field measurements appear simpler at the present time and also have given results much more consistent with theoretical estimates. In addition, for application to environments where high-impedance techniques cannot be used, testing was begun on low-impedance sensors in this program as a first step in interpreting the data in terms of the strong interaction between sensor and environment. It is felt that the sensors and accompanying technological advances from this program will allow acquisition of excellent diagnostic ancillary data for such important tests as weapon-system IEMP, satellite SGEMP (system-generated EMP) and transmission-line coupling.

# III ANALYSIS

In this section, simple analysis is used to provide estimates of the potentials and fields generated in the various machine and cavity environments and a description of the sensor response and the factors affecting it. It will be seen that the characteristics of the driving charges (or currents) and the resulting state of the environment has a profound effect on both the magnitude and the time variation of the fields produced, and also upon the sensor response to the fields.

## A. Estimates of Potentials and Fields--Neutralization by Air Ionization

When there is no air present, the fields result entirely from the space charge consisting of the Compton electrons and photoelectrons scattered out of the cavity walls. However, when air is present, it becomes partially ionized by the photons and by electrons produced in these and subsequent collisions with the air molecules. If the resulting plasma conductivity builds up to a high enough value during the pulse, the Compton-generated fields will cause significant currents in this plasma that result in neutralization of the potential in a manner similar to relaxation of charge density in a conductor. For the case of the IEMP field, where the presence (rather than movement) of the source electrons is the source of the electric fields, the low-energy electrons are swept toward the wall by the space-charge fields, leaving the less mobile positive ions essentially fixed in the cavity. If there is sufficient plasma density and enough time for this process to occur, these currents will flow until there is a sufficient excess of the low-energy positive ions to nearly neutralize the high-energy driving electrons, and therefore to nearly neutralize the space-charge source of the fields. For the EMP-type fields where there is no net space charge (see Figure 4), the movement of the source electrons (Compton currents) is the field source. In this case, the neutralization phenomenon is caused by the low-energy electron currents flowing opposite the Compton currents. In either case, it is shown in Appendix A that the neutralization occurs in a characteristic time similar to the well-known charge-relaxation time $\tau = \epsilon_o/\sigma$ in conducting media. It is seen that these times are high compared with Febetron 706 pulse duration, but can and do occur during the longer Febetron 705 and Aurora pulses.

In Appendix A, we determine electron, positive-ion, and negative-ion densities for a dose rate increasing linearly with time, which is appropriate for the leading edge of the pulses of all three machines. These densities are shown in Figure A-1 of Appendix A normalized by the slope of the dose rate. Using these values, we proceed to solve for the fields and neutralization times for the free-field (EMP) case. An important result of this analysis is the prediction that the maximum field produced in the Aurora free-field regions will be 17 kV/m to 60 kV/m, where this range of the predicted values depends on the value of electron mobility used in the calculation.

A corresponding analysis of neutralization times and peak fields and potentials for the bounded (IEMP) case is also given in Appendix A. In both EMP and IEMP cases, the neutralization times, and therefore peak fields, are seen to be complicated functions of the dose rate. These functions have different forms, depending on whether the neutralization occurs in times short or long compared with characteristic electron attachment times.

## B. Sensor Response

An open-circuited grid that has no net charge resides at the potential created by its space-charge environment; however, there are a number of competing physical processes that can cause charge buildup on the grid. When this occurs the grid potential is shifted and the environmental potential is not directly measured. The effect of charge deposition on the potential of an open-circuit grid is depicted in Figure 5. The grid is located between two ground planes in a negative-space-charge-potential distribution (solid curve). The dashed curve illustrates how deposition of positive charge on the grid can shift its potential. The charge imbalance creates a new potential distribution that may in turn modify the intrinsic space-charge environment that is to be measured.

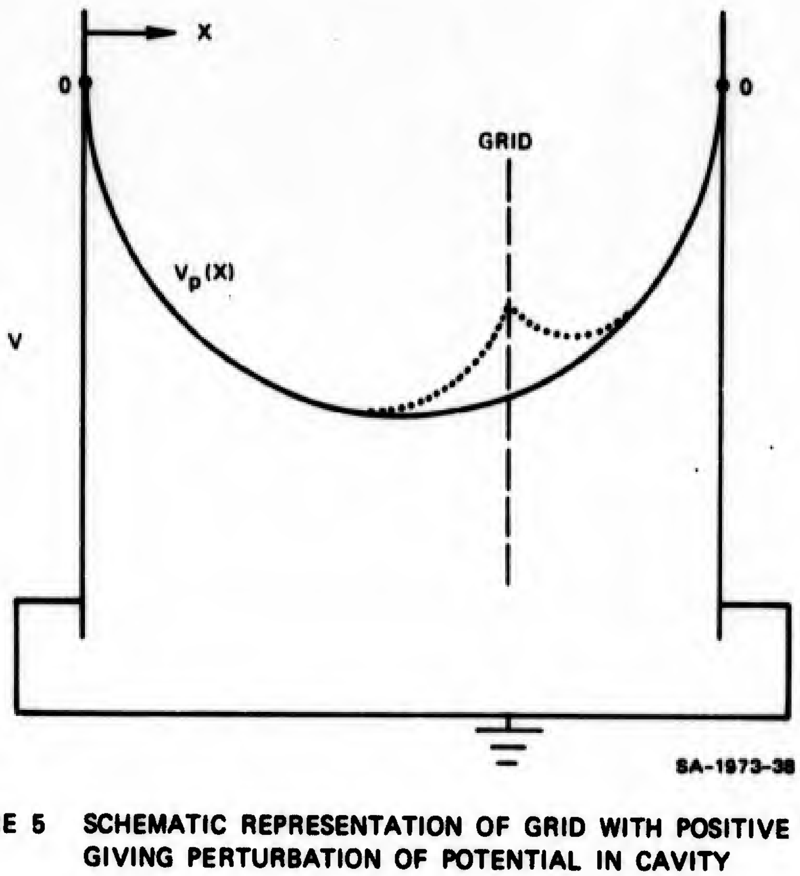


FIGURE 5 SCHEMATIC REPRESENTATION OF GRID WITH POSITIVE CHARGE, GIVING PERTURBATION OF POTENTIAL IN CAVITY

Appendix B gives a brief analysis of these phenomena, culminating in a description of the sensor response in the IEMP case. A corresponding lumped-circuit analog for the analysis is shown in Figure 6. A series

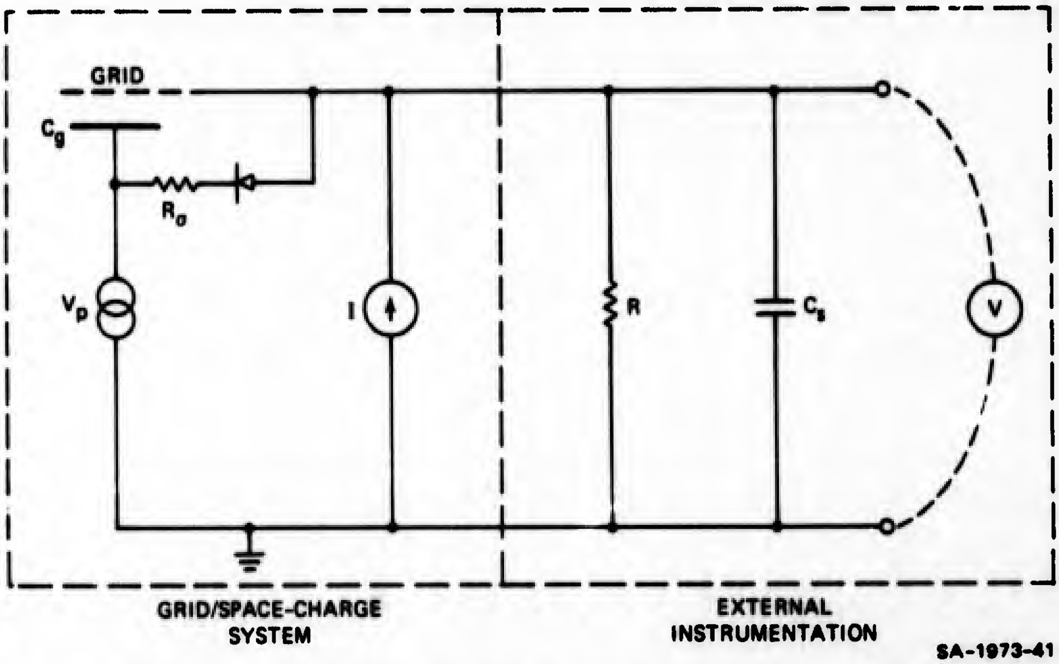


FIGURE 6 ELECTRICAL ANALOG OF SENSOR/SPACE-CHARGE SYSTEM WITH LOAD CIRCUIT

of measurements was made using an actual electronic circuit similar to that of Figure 6 to demonstrate the various pulse shapes that can be produced by this kind of circuit and to predict the results of the flash X-ray-machine measurements. The agreement between the predicted pulses and the actual machine-produced potentials confirms the circuit of Figure 6 as a valid analog for the grid/environment system.

# IV DESCRIPTION OF APPARATUS AND ENVIRONMENTS

## A. Febetrons

The Febetron 706 tests were performed on the Febetron 706 at Stanford Research Institute. The 705 tests were performed on the 705 at the Air Force Weapons Laboratory and were supported by DNA. In addition to the properties mentioned in Table 1, normalized photon spectra of the two machines are given in Figure 7. Plotted on the same abscissa and with atomic number as the ordinate are the regimes where the three principal photon interactions are dominant.

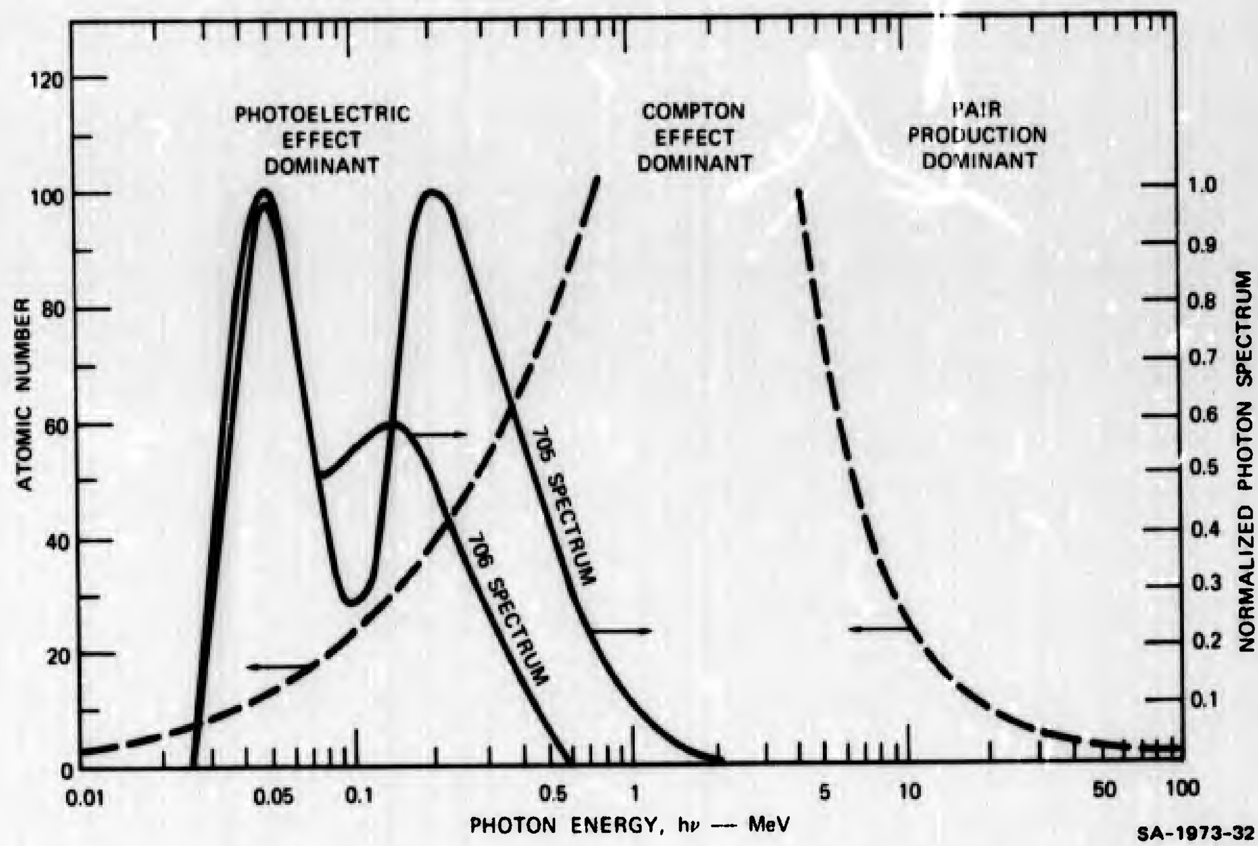


FIGURE 7 NORMALIZED PHOTON SPECTRA OF 705 AND 706 FEBETRONS, SUPERIMPOSED OVER MAP OF DOMINANT PHOTON INTERACTION REGIMES AS A FUNCTION OF ENERGY AND Z OF INTERACTING MATERIAL

The grid/cavity systems shown in the lower-left corners of Figures 2 and 3 were used with both Febetrons. Three configurations were used:

(1) The vacuum-tight aluminum shell shown in Figure 3, with both grids at fixed locations, and a 2.5-cm separation between the plates.

(2) A room-pressure shell with one fixed grid and one grid movable (by virtue of a micrometer head) over a 0.8-cm range, and a 2.5-cm separation between plates.

(3) A modification of (2) with the removal of the fixed grid and installation of the emission plate closer to the end target, allowing the movable grid to scan almost the entire cavity from plate to plate.

Lead collimators with a 1-cm-diameter hole were used.

In the 706, the conduction (low-energy) electron density is calculated to be typically $10^8$ or $10^9$ el/cm$^3$ during the pulse, depending on the local dose rate. Since the characteristic attachment time is about 10 ns, the electrons essentially accumulate throughout the 3-ns pulse, and they are converted to negative ions by attachment to oxygen molecules after the pulse. In the 705, the electron density was calculated to reach up to $10^{11}$ el/cm$^3$, peaking during the second half of the pulse. The electron decay relative to the pulse duration is quicker in the 705 than in the 706.

One of the grid configurations used frequently in the Febetron tests is drawn in Figure 8. To accentuate the charge-deposition effect, this design was later modified such that all the elements were 10 mils wide. In addition, sensors of the same basic outline were made of aluminum honeycomb (holes parallel to the flux) and of solid foils of several metals.

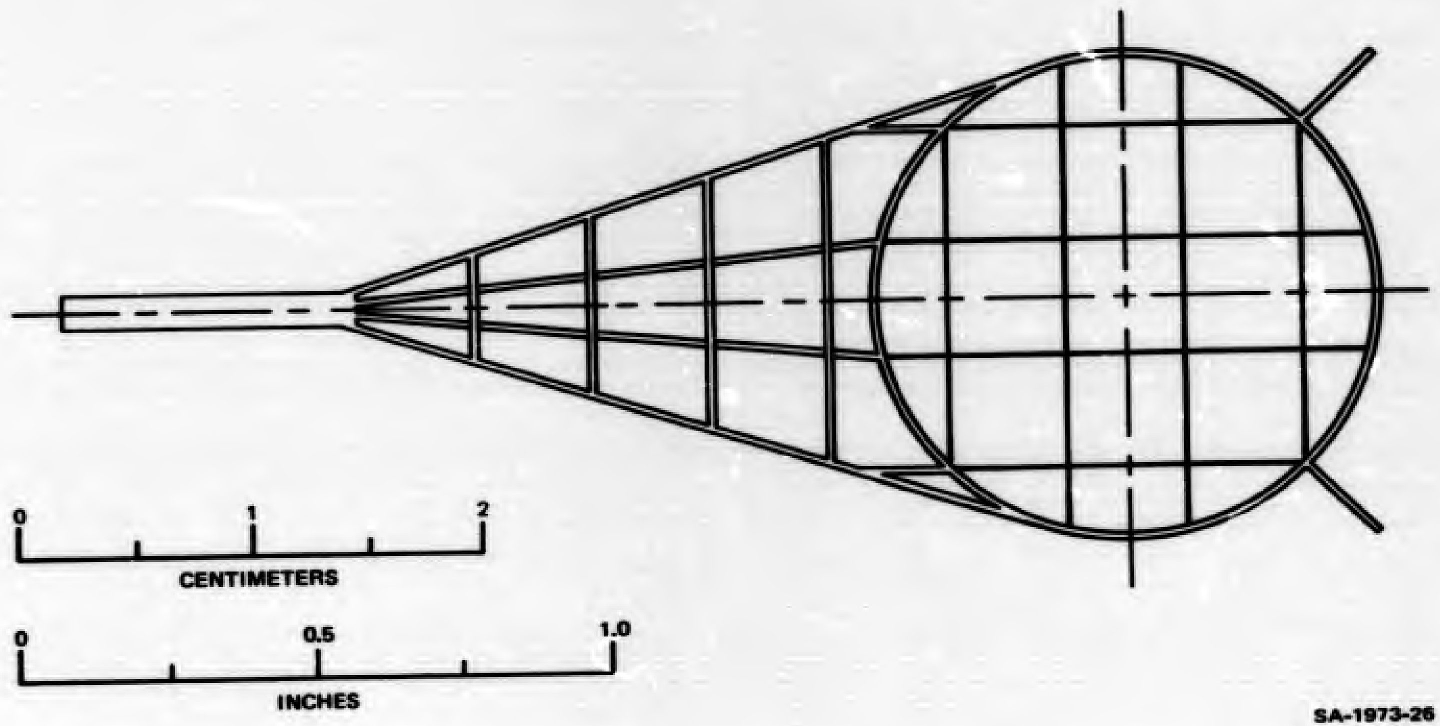


FIGURE 8 SENSOR MESH PATTERN

Various load resistors and high-impedance voltage probes were used in the Febetron tests. The HP Model 1120A FET probe with an input impedance of 1 MΩ was used for most of the true open-circuit voltage measurements. However, this probe was found to be subject to TREE upsets in the 705 when it was attached to the connectors shown on the cavities (Figures 2 and 3). Thus, a one-foot length of RG-58 cable was used so that the probe could be remoted and shielded. This cable added shunt capacitance to the system and caused some observable ringing in the monitored signal.

High-bandwidth oscilloscopes such as the HP 183 and Tektronix 454 were used for the 706 work, and Tektronix 7704s were furnished at the AFWL 705.

## B. Aurora

The spatial characteristics of the Aurora beam are complex, since there are four guns directed toward a "hot spot" in the test cell. A dose exceeding $4 \times 10^4$ rad is delivered to the hot spot of about 20-cm diameter. A detailed description of the radiation levels and of the Aurora facility in general is given elsewhere[5] and will not be repeated here. Figure A-1 of Appendix A shows calculated (normalized) electron and ion densities for the first 80 ns of the Aurora pulse, after which the photon pulse rounds off from the nearly linear rise. The measurements were made in a series of fifteen shots, using the array of grid/plate assemblies shown in Figure 2 housed inside a double-shielded metal cassette, which is depicted in Figure 9. As is recommended for minimizing noise reaching the data room, the inner metal cassette was joined to the data room by a shielded zip tube, inside which were the bundled cables leading from the cassette to the data room and eventually to the 28 data-recording channels (Tektronix 556 and 7703 oscilloscopes). Then the outer cassette was joined by a second zip tube, which shielded the first tube (but was dc-isolated from it) and was joined to the test cell walls. The test cell is a completely enclosed metal room, 15 by 48 by 65 feet, which very effectively shields out the Aurora machine noise. The double cassette was divided into two compartments, separated by a one-inch-thick aluminum bulkhead. The grid array and the vacuum chamber, when used, were located in the upper chamber. Fine-wire insulated leads (0.0044 inch diameter) were connected from the grids to pass-through connectors in the bulkhead, and thence to the amplifiers in the lower compartment just beneath the bulkhead. The lower compartment was shielded from the photons and scattered electrons by several inches of lead all around the outside and on the aluminum bulkhead. The vacuum

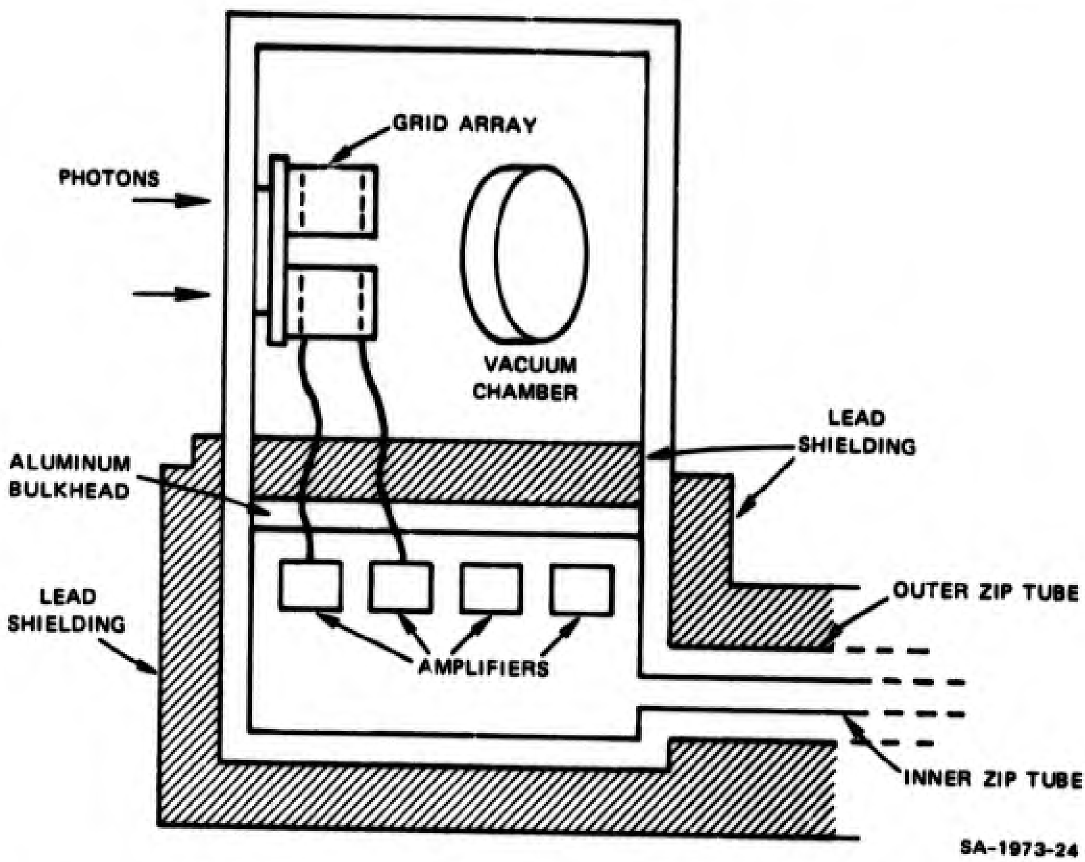


FIGURE 9 DOUBLE-CASSETTE SHIELDING SETUP DEPICTING GRID AND AMPLIFIER LOCATIONS

chamber was closed off and disconnected from the pump just before each shot.

The cassette was placed with the grid array approximately 50 cm from the hot spot to achieve a nearly homogeneous dose over the array. The grid array shown in Figure 2 used rectangular mesh grids of either aluminum or copper. Grid spacing from the emission plates could be varied arbitrarily up to 7 inches. The emission plates and end targets were made of aluminum, copper, tin, or lead. The vacuum-chamber materials, including the larger grid, were all aluminum.

Four pass-through connectors were placed in the lower compartment walls to allow measurements outside the double cassette. Fine-wires (0.0044 inch diameter) were run to pairs of parallel grids placed one to three inches apart to make field measurements two or more feet from the cassette.

The amplifiers had a voltage gain of approximately 0.5, with provision to capacitively divide the signal by 10:1 or 100:1 ratios using two 10:1 stages. The input impedance without voltage dividers was $10^5$ ohms, and with one or both divider stages it was $10^7$ ohms.

V RESULTS OF MEASUREMENTS

## A. Febetron 706 Data

Figure 10 shows examples of potential measurements from the 706 with two different grid-material, end-target, and emission-plate

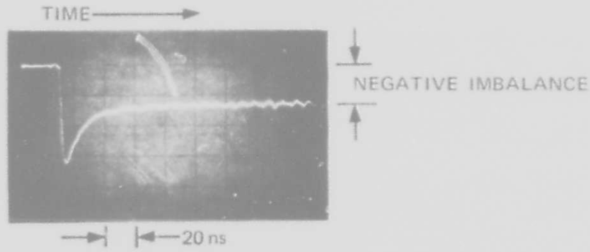


(a) Al GRID, Be EMISSION PLATE, Ta TARGET

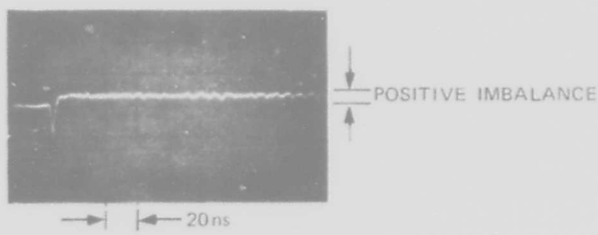


(b) Cu GRID, Be EMISSION PLATE, END TARGET REMOVED

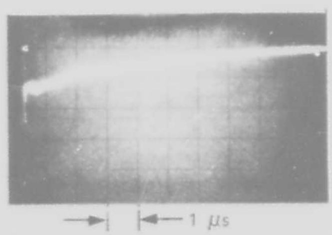


(c) SAME AS (a) EXCEPT CONTRACTED TIME SCALE

SA-1973-35

FIGURE 10 EXAMPLES OF MEASURED OUTPUT VOLTAGE FROM FEBETRON 706 TESTS (RC >>> $\tau_p$)

combinations, using RC >>> $\tau_p$, where $\tau_p$ is the pulse duration. It is seen that the net charge deposition (imbalance) was negative for Figure 10(a) and positive for 10(b). The data from these figures, by use of Eq. (B-14), give the actual peak space-charge potential. In Figure 10(a) the peak potential is just slightly greater than the peak indicated, since the imbalance error is quite small. It is interesting to note that the pulse in Figure 10(a) requires about 25 or 30 ns to round off to the imbalance level. This is believed to be a result of the stopping of the soft photoelectrons from the tantalum end target by the air (at one atmosphere), followed by a relatively slow relaxation of this stopped charge after the pulse has ended. The most likely mechanism for this relaxation is the residual conductivity of the low-energy free electrons (plasma electrons). The much longer RC decay of the deposited charge is shown in Figure 10(c), which has a much slower sweep speed.

A summary of the imbalance voltage found as a function of grid, emission plate, and end-target materials is given in Section VI.

B. Febetron 705 Data

Figure 11 shows an example of an open-circuit-voltage measurement with the 705. The ringing that is readily apparent in traces like this is apparently due to the foot-long cable between the grid and the amplifier that was needed to get the amplifier shielded from the radiation effects. The ringing did not occur when such cables were not used.

Figure 12 shows two examples of the measured peak potentials (negative) in the 705 as a function of distance, using a grid in the micrometer head.

Imbalance voltages were measured in the 705 using 3%-opacity, 5-mil-thick aluminum and copper grids, for emission plates with two different atomic numbers, Z, and four different end targets. These data are summarized in Section VI.

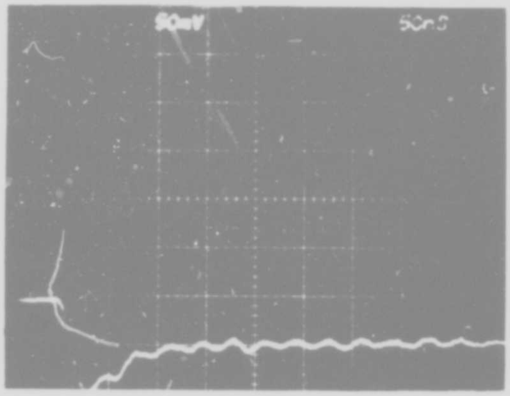


SA-1973-27

FIGURE 11 EXAMPLE OF OPEN-CIRCUIT DATA FROM FEBETRON 705 (Cu grid, Al plate, Ta end target)

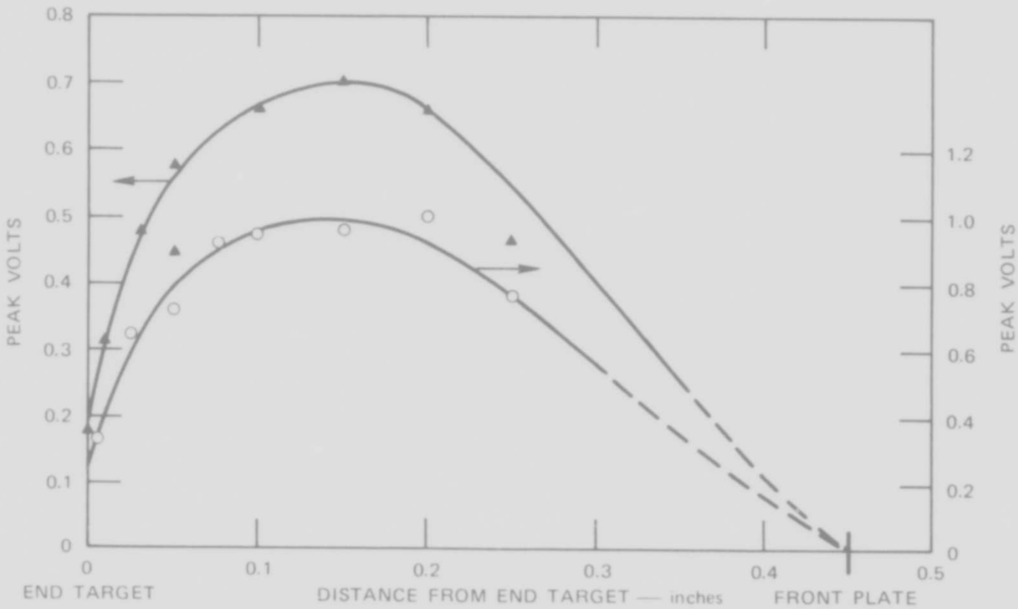


SA-1973-30

FIGURE 12 EXAMPLES OF MEASURED POTENTIAL PROFILES IN THE FEBETRON 705

Another test performed in the 705 was an attempt to determine the effect of spectrum hardness on the imbalance voltage. The 705 spectrum was "softened" somewhat, compared with Figure 7, by decreasing the maximum voltage from 2.0 mV to 1.4 MV. Then the spectrum was hardened by using the maximum voltage of 2.0 MV along with a ¼-inch lead plate to filter out X-rays on the low-energy side. Although the doses ended up to be approximately the same in both cases, the voltages were normalized by the total dose and are given in Figure 13 for an aluminum grid and copper emission plate as a function of three values of end target Z. The trend toward a less serious imbalance or charge-deposition problem in the case of harder spectra can be seen in Figure 13.

Many other grid variations were run with the Febetron 705. It was found that the imbalance voltage was indeed proportional to opacity of 10% and less. For solid-foil "grids," the imbalance voltage was still higher, though not quite proportionately higher, perhaps because the grid with 100% opacity is imposing enough to significantly perturb the environment it was intended to measure. In another attempt to "match" the grids to the environment, two-layered grids were used, with each layer of a different metal, such that the forward-scattering layer would be matched (same Z) to the emission plate, and the backscattering layer would be matched to the end target. Probably because of air effects and beam divergence, this did not achieve as good a charge balance as expected. A grid configuration of aluminum honeycomb, oriented with high transparency to the flux direction, was used to determine if an increase in grid capacitance could be effected with less than a proportionate increase in the charge deposition. However, a large proportion of charge deposition was measured.

## C. Aurora Data

Data were taken with many combinations of emission plates, grids, and end targets in Aurora, but only slight variations occurred in the

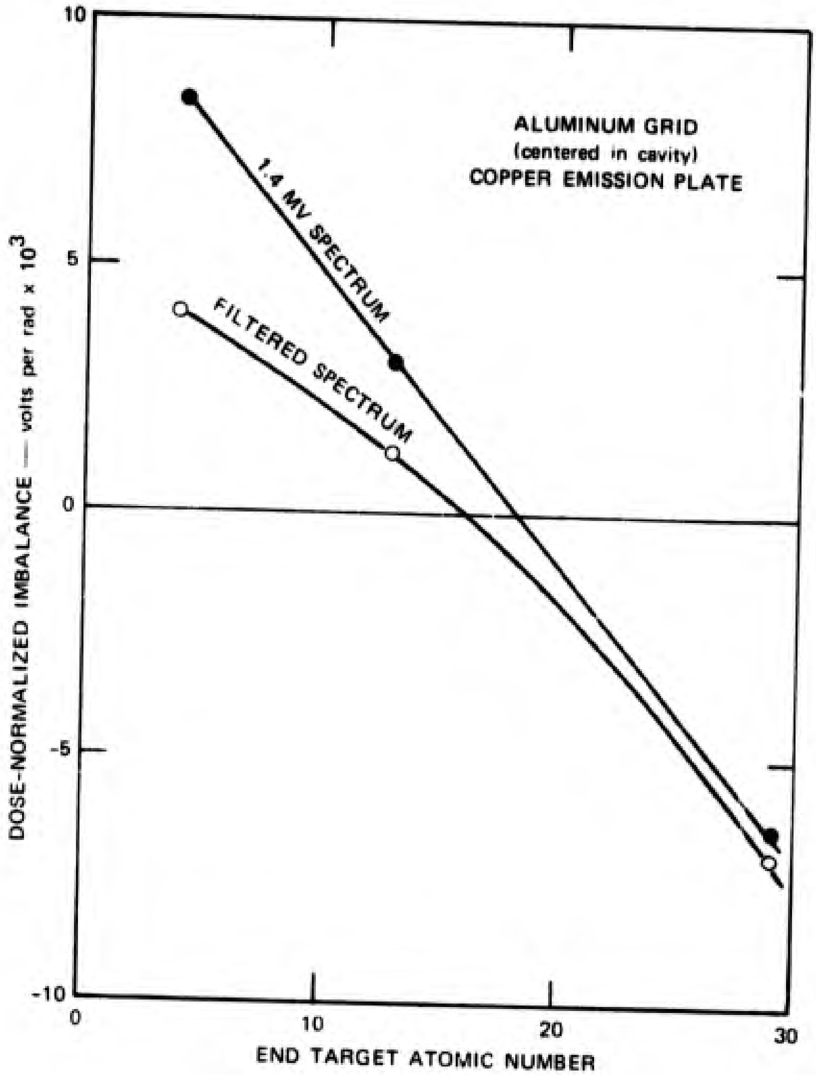


SA-1973-33

FIGURE 13 EFFECTS OF X-RAY SPECTRUM ON IMBALANCE VOLTAGE (FEBETRON 705)

results, whereas large variations were found in the Febetron data. In fact, no imbalance data were apparent in the traces. This is apparently due to the continuous action of the high-conductivity plasma ($\sim 5 \times 10^{-2}$ mho/m) in neutralizing any charge deposition on the grid that would cause the grid to have a potential different from the local potential. Any tendency of the grid to acquire a net positive charge (as depicted in Figure 5) would cause it to draw a compensating electron current from the surrounding plasma. Similarly, excess electrons on the grid would cause the grid to draw positive-ion current, the greater density of which somewhat compensates for the lower mobility of the ions.

Figure 14 shows some of the results of data taken to determine the noise levels under various conditions. It can be seen that the most severe noise condition is about a 0.3-volt accumulated upset of an open-input amplifier with a 10:1 divider and a (typical) dose of 10 R. The long-term deviation of this upset is demonstrated by the lower trace of Figure 14(d). On the other hand, the upper trace of Figure 14(b) shows a negligible upset with a 20-R dose with a 50-ohm input. The lower trace of Figure 14(b) shows the effectiveness of the double-cassette/zip-tube shielding scheme in suppressing pickup on cables.

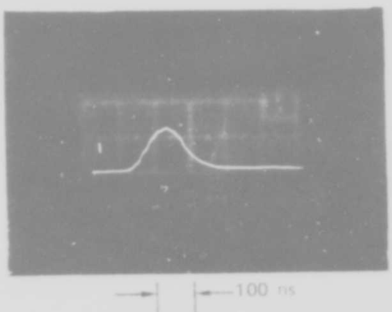


(a) AURORA PHOTON PULSE

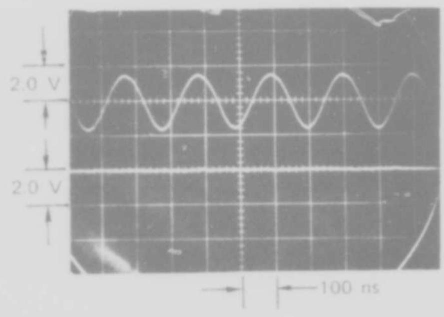


(b) UPPER TRACE: 5 MHz SIGNAL THROUGH AMPLIFIER (dose = 20 rad)
LOWER TRACE: NOISE ON RG-58 CABLE DISCONNECTED AT AMPLIFIER END

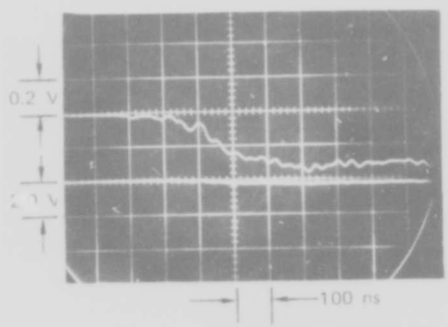


(c) BOTH TRACES: TREE NOISE FROM AMPLIFIER ON 10:1 DIVIDER, NO INPUT (dose = 10 rad)

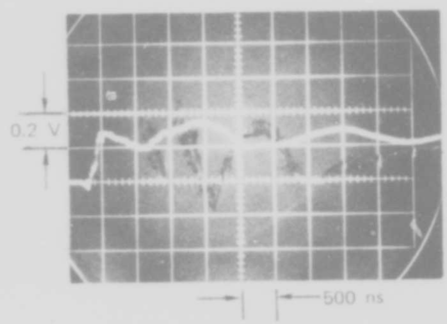


(d) LOWER TRACE: DEMONSTRATION OF LONG DURATION (> 5 μs) OF TREE EFFECT FOR OPEN AMPLIFIER

SA-1973-36

FIGURE 14 NOISE-LEVEL MEASUREMENTS FOR AURORA TESTS

Figure 15 shows several traces of the potentials measured in the grid/plate array at various spacings between the 6-inch-separated plates. The vertical scales given in brackets allow a reading of the actual potential of the grids, taking into account the amplifier gains and the small amount of cable loss. Figures 15(c) and 15(d) are shown to indicate the total duration of the measured signal, which is seen to be greater than the Aurora pulse duration but less than the duration of the TREE effect on the amplifier [Fig. 14(d)]. The magnitude of these signals is seen to considerably exceed the TREE-effect noise of approximately 0.3 volts.

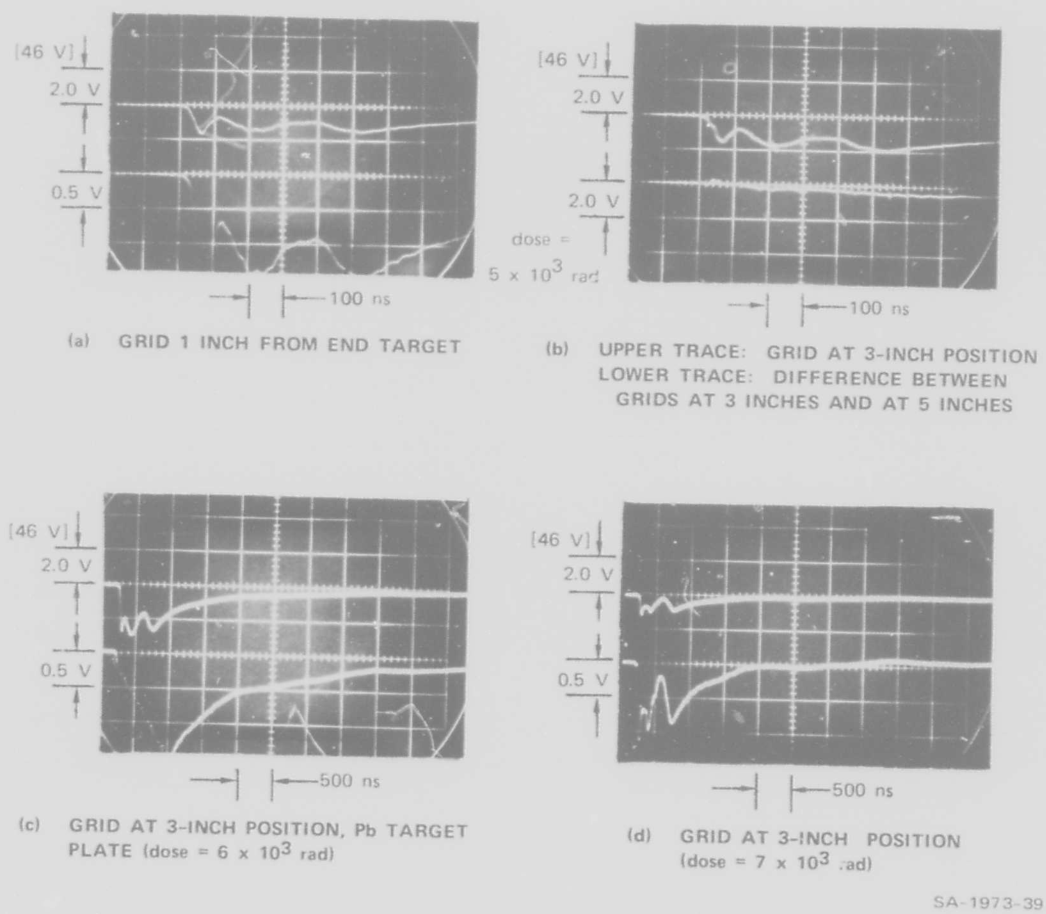


(a) GRID 1 INCH FROM END TARGET

(b) UPPER TRACE: GRID AT 3-INCH POSITION
LOWER TRACE: DIFFERENCE BETWEEN GRIDS AT 3 INCHES AND AT 5 INCHES

(c) GRID AT 3-INCH POSITION, Pb TARGET PLATE (dose = $6 \times 10^3$ rad)

(d) GRID AT 3-INCH POSITION (dose = $7 \times 10^3$ rad)

SA-1973-39

FIGURE 15 GRID POTENTIALS IN 6" CUBICLES AT ONE ATMOSPHERE

Figure 16 shows the potentials in the vacuum chamber for four different pressures. In this chamber, the grid is centered between plates separated by 2 inches. These potentials come closer to reproducing the photon pulse shape than the 6-inch separation measurements of Figure 15.

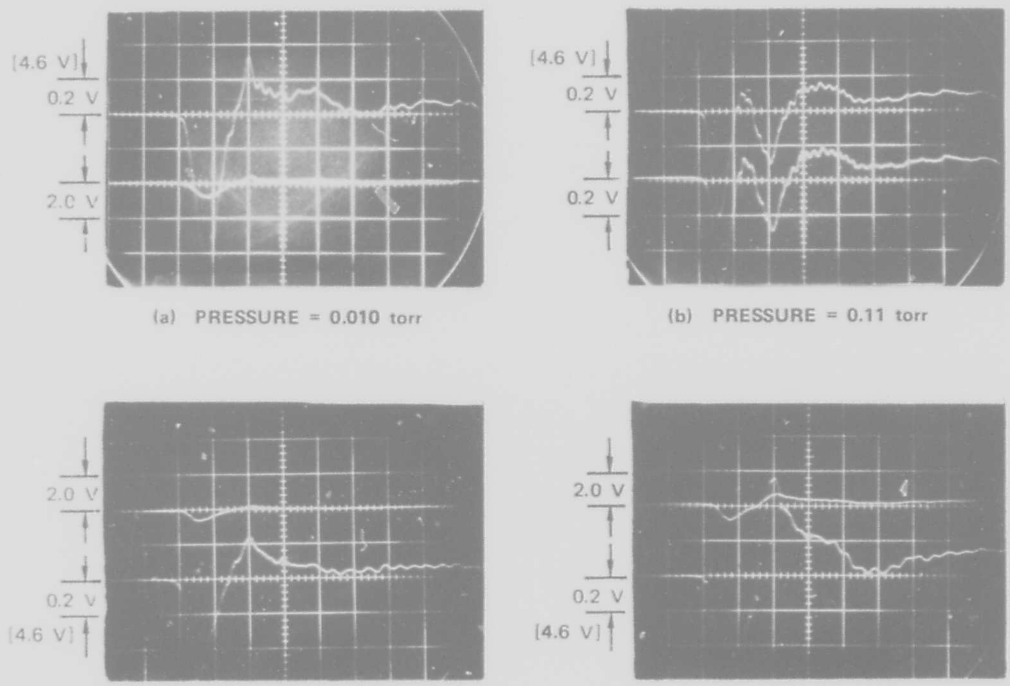


(a) PRESSURE = 0.010 torr

(b) PRESSURE = 0.11 torr

(c) PRESSURE = 1.0 torr

(d) PRESSURE = ONE ATMOSPHERE

SA-1973-42

FIGURE 16 VACUUM CHAMBER POTENTIALS

Figure 17 shows that even a sensor made of solid aluminum foil shows negligible charge-deposition effects. However, the solid tantalum foil gives a strong positive-charge-deposition result, going off-scale in the (expected) positive direction.

Electric field measurements were performed outside the double cassette by taking the difference of open-circuit potential between pairs of parallel grids. One pair, separated by one inch, was placed

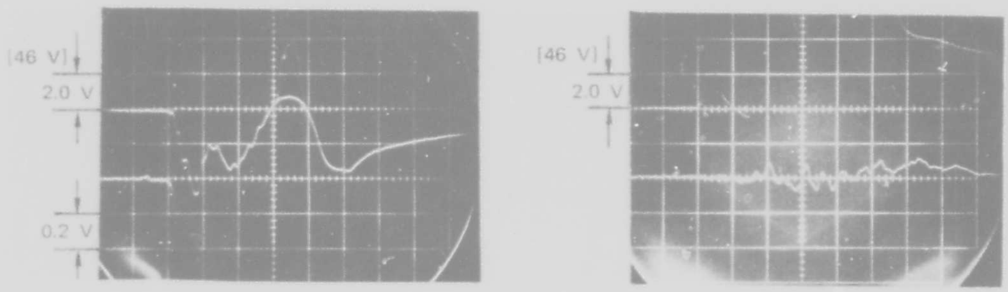


(a) 2-mil ALUMINUM AT 2-INCH POSITION

(b) 2-mil TANTALUM (upper trace only) AT 2-INCH POSITION

SA-1973-22

FIGURE 17 MEASUREMENTS WITH SOLID-FOIL "GRIDS" IN 4" CUBICLES

in a high-dose region ($3.5 \times 10^3$ rad) off to the side of the hot spot, supported on a dielectric stand. The potentials are shown in Figure 18(a) and their difference in Figure 18(b). The maximum difference is seen to be about 100 volts, giving a field strength of about 4 kV/m. The common-mode-rejection ratio of these measurements was about 40 dB in tests made in a non-radiation environment. However, there may be additional error associated with the leads crossing equipotentials during the pulse, although for this particular pair of grids the 3-foot-long leads were nominally parallel to equipotentials. A second pair of grids, 3 inches apart and connected to the cassette by leads approximately 5 feet long, was placed in a lower-dose area in a region shielded by the lead-shrouded lower cassette. The measurements made using these grids are shown in Figures 18(c) and 18(d). The difference, which looks qualitatively quite different from the other result, has a peak of about 1000 volts for 3-inch separation, corresponding to a peak field of about 13 kV/m. Although this value agrees better with theoretical predictions, the orientation of the 5-foot leads approximately parallel to the Compton currents suggests more possible error in this location. Figure 18(e) shows the difference measured by a 600-ohm balun transformer, giving a peak measured field strength of only 130 V/m.

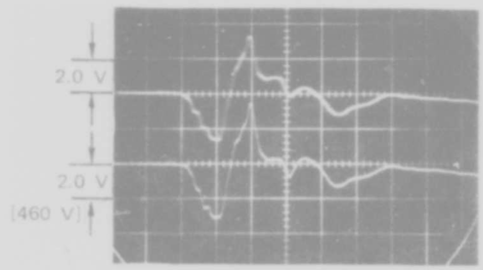


(a) POTENTIAL OF INDIVIDUAL GRIDS, 1-INCH SEPARATION (upper trace, grid near source)

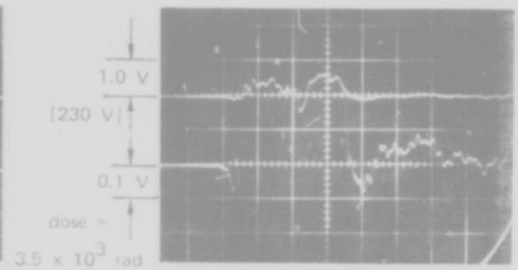


(b) DIFFERENCE IN POTENTIALS SHOWN IN (a).

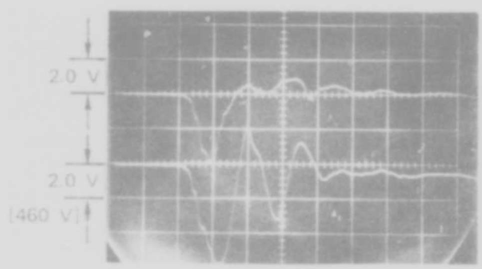


(c) POTENTIAL OF INDIVIDUAL GRIDS, 3-INCH SEPARATION (upper trace, grid near source)

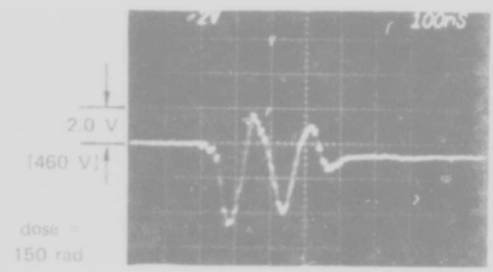


(d) DIFFERENCE IN POTENTIALS SHOWN IN (c)

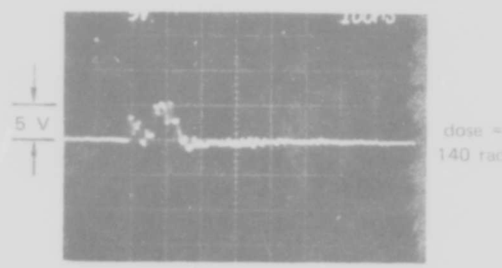


(e) GRIDS WITH 3-INCH SEPARATION, DIFFERENCED THROUGH 600-$\Omega$ BALUN

SA-1973-25

FIGURE 18 "FREE-FIELD" MEASUREMENTS

Appendix C gives some examples of data from other types of tests made in Aurora, especially those using low-impedance devices.

## D. Discussion of Aurora Data

Although from an experimental standpoint there is every reason to confirm that the grid/amplifier combinations correctly measured the electric potentials in the Aurora tests, the results do not all agree with the rather simple theoretical analysis performed in support of the tests. For instance, it was expected that in high-dose regions the potentials would reach a peak much earlier than the peak dose rate due to neutralization, and this occurred in every case. However, the time required to reach peak appears to be 30 to 40 ns, whereas the analysis in Appendix A predicts 8 to 10 ns. Since the time appears to be longer, it would be expected that the measured peak potentials would be higher than predicted, which were 100 to 140 volts for a grid centered in a 6-inch cubicle and 10 to 15 volts typically in the 2-inch cubicles. However, the measured results gave 30 to 60 volts typically in the 6-inch cubicles. The 2-inch vacuum chamber gave approximately 15 to 20 volts at all four pressures, although it is noted that the potential peaked 60 to 70 ns into the pulse at the lowest pressure (0.01 torr). The unknown shunt capacitance of leads, etc., could be dividing down the potentials, especially in the 6-inch cubicle where the grid capacitance is approximately one-tenth that of the vacuum chamber grid. The temporal behavior of the potential following the peak is not understood, and since the analysis applies only to a linearly increasing dose rate, it is not applicable beyond about 80 ns into the pulse. The measured potential typically has three maxima (negative) in the 6-inch and 4-inch cubicles, and was seen to occasionally go to positive potentials on the second positive-going swings, which occurred after the radiation pulse was ended. In the low-pressure and free-field measurements, the positive swing always occurred, however, and it did so during the photon pulse. The frequency of the undulations in the potential does not appear to be related to the ion resonance frequency, which is about $10^8$ Hz for $n_+ = 5 \times 10^{18}$ $m^{-3}$. The duration of the space-charge potential well after the photon pulse is ended is apparently related to the abundance of positive and negative ions, and the time for the potential to decay after the pulse appears in reasonable agreement with recombination rates and the maximum density of the ions. For the high-dose-rate regions (~$6 \times 10^3$ rad), $n_+$ and $n_-$ are expected to reach approximately $5 \times 10^{18}$ $m^{-3}$, and the recombination coefficient is thought to be $2 \times 10^{-12}$ $m^3/s$, indicating ~300 ns as the time for the ion density to decay to one-fourth its maximum value. This value is in good agreement with Figure 15(d) but in only fair agreement with 15(c).

It is seen that there were no observable imbalance potentials, but the neutralizing action of the highly conductive plasma in Aurora appears to prevent significant accumulation of imbalance charges on the grids. This phenomenon was observed in the highly conductive plasma produced by the Febetron 706 in the electron mode. Additionally, the nearly complete insensitivity of the peak potential to the grid and plate atomic numbers (only a lead end target affected it) supports the belief that charge deposition is not significant in Aurora measurements with grids of 3% opacity. In addition to the plasma neutralization, it is believed that other factors contributing to low imbalance potentials are: (1) the 5-mil grid thickness is a much lower fraction of Aurora mean electron range, and (2) photoelectron scattering, which is a strong function of atomic number, is quite reduced compared with Compton scattering for this spectrum.

## VI RESULTING SENSOR/SYSTEM DESIGN CRITERIA

In this section we discuss various design criteria for a sensor and associated circuitry. Some of these criteria have evolved from the tests made during this program, but some constraints that were obvious before the study began are also included. Earlier treatments of this subject are recommended.[6,7] Since only the open-circuit-voltage measurement with fine-wire grids is well understood, we will limit this section to a discussion of such a measurement that is designed for operation in its specific environment.

### A. Configuration and Dimensions

It is obvious that the volume of the grid material per unit area should be minimized, since the absorption of electrons and the cross-section for photon interaction are a function of the volume. However, it is shown here that, due to practical considerations, there is usually a constraint relating volume to opacity. It would be worthwhile to differentiate between (a) the "wire" dimension parallel to the nominal direction of the photon and electron beams, and (b) the dimension transverse to this direction, except for two practical considerations:

(1) The beams are not actually unidirectional.

(2) The wires of interest are often so small that it is difficult to fabricate them with the "parallel" dimension any smaller than the transverse dimension--i.e., they usually approximate a circle (or square) in cross section.

Thus, only wires, or elements with dimensions equal in the two directions, are considered for mesh construction. A good standard fabrication technique for elements as small as 3 mils is printed-circuit etching. It also turns out that dimensions of the order of a few mils are sufficient to make the wire radius greater than one skin depth for the response to the lowest frequency of interest (Aurora's 250-ns pulse). A consideration of high-frequency response requires that the largest dimensions of the entire grid be small compared with the "signal transit distance" $c\tau_{min}$, where c is the speed of light and $\tau_{min}$ is the minimum time interval of interest, typically the pulse rise time. To avoid retardation effects, the same constraint is placed on the largest dimension of the grid cavity. On the other hand, the grid must be large enough to give the desired capacitance, C, which will be discussed in connection with the external circuitry, in Section VI-C.

Since it is assumed that the "wires" are approximately circular in cross section, opacity of the grid (defined as the ratio of the projected area of the wires to the total area of the grid) will be a measure of the actual volume of the grid material. The opacity is given approximately by $4r_o/b$, where $r_o$ is the wire radius and b is the wire-to-wire spacing. The upper limit of b comes at approximately the spacing, d, between the grid and the plates, since the capacitance between the grid and a plate no longer approximates that of a solid plate when $d \lesssim b$. Typical minimum opacity with the printed-circuit etching technique is 2% to 3%. However, a special process developed at the Air Force Weapons Laboratory has produced opacity lower than one percent.[8]

In summary, the opacity, $4r_o/b$, should be minimized. The limitations, other than the state of the art in manufacturing, are:

(1) $r_o$ should not be reduced sufficiently to give enough impedance on the wire for currents flowing across the grid to the load to generate a significant potential difference (compared with potentials being measured). Thus, considerations of the skin depth for the frequency spectrum of interest will have to be considered.

(2) b should not exceed d since the capacitance of the mesh to a plate is reduced significantly beyond this point.

B. Noise Signal From Charge Deposition

Section III describes a method for discriminating between the unwanted contribution of charge deposition to the grid voltage, and the desired local potential. However, this discrimination is not practicable if the signal-to-noise ratio degrades below 1/3 or so, and data from both Febetrons show cases when this ratio goes well below 1/3 with grids of opacity around 3%.

Thus it appears that attention must be given to choosing an appropriate grid material, especially in beams with spectra as soft as those of the two Febetrons, unless the conduction plasma density is high enough to continually oppose the charge accumulation. The results of measurements of imbalance voltage in the parameter study in the two Febetrons can be used as an empirical guide for selection of grid material. These results are summarized in Figure 19, for the Febetron 706 data, and in Figures 20 and 21 for the Febetron 705.

Now, it might be expected that if a grid stops most of the source electrons impinging on it (which happened even with a 5-mil-thick aluminum grid as Febetron 705 tests showed), then a grid with atomic number $Z_1$ would be balanced when both plates are made with the same material. This balance would result because the grid would absorb an electron from the emission plate for every electron the grid emits forward, and it would absorb one incident from the end target for every one it backscatters. The measured results show that this is not quite the case, but it is usually close enough to it so that the signal can be discriminated from the noise.

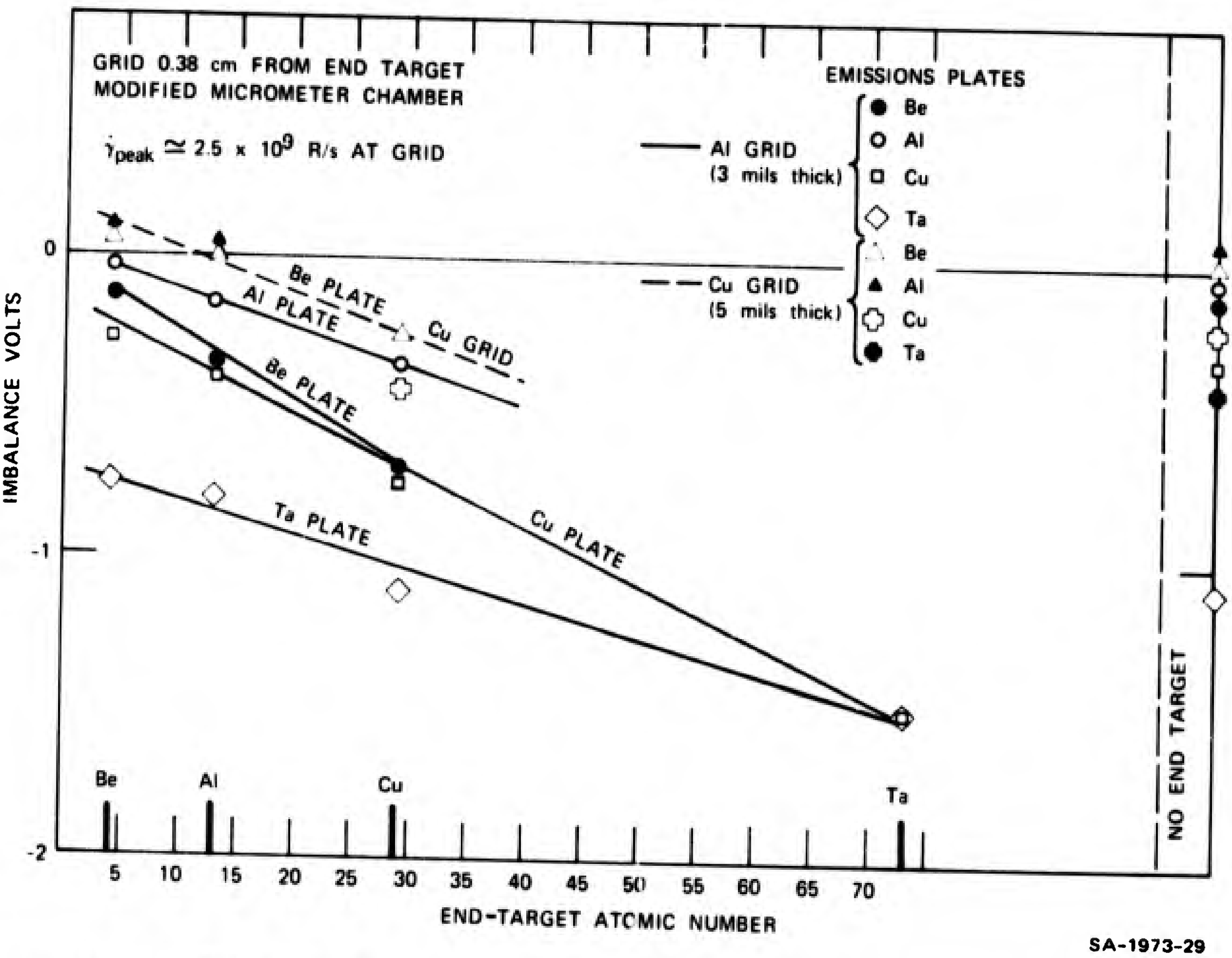


FIGURE 19 IMBALANCE-VOLTAGE DATA FROM 706 TESTS AS A FUNCTION OF END-TARGET ATOMIC NUMBER AND GRID AND EMISSION-PLATE MATERIALS

Similarly, it appears that if the plates are made of different materials, then a grid with a Z intermediate between the two materials would be usable, as demonstrated by Figure 10(a) for an aluminum grid with a beryllium emission plate and tantalum end target in the Febetron 706. Figure 11 shows a similar result for a copper grid between aluminum and tantalum. In both of these cases, it appears that a grid with somewhat higher Z would give still higher signal-to-noise ratio, probably near the arithmetic mean between the atomic numbers of the two end plates.

If a sufficiently high plasma conductivity is predicted, then the selection of grid material is less critical. However, it should be

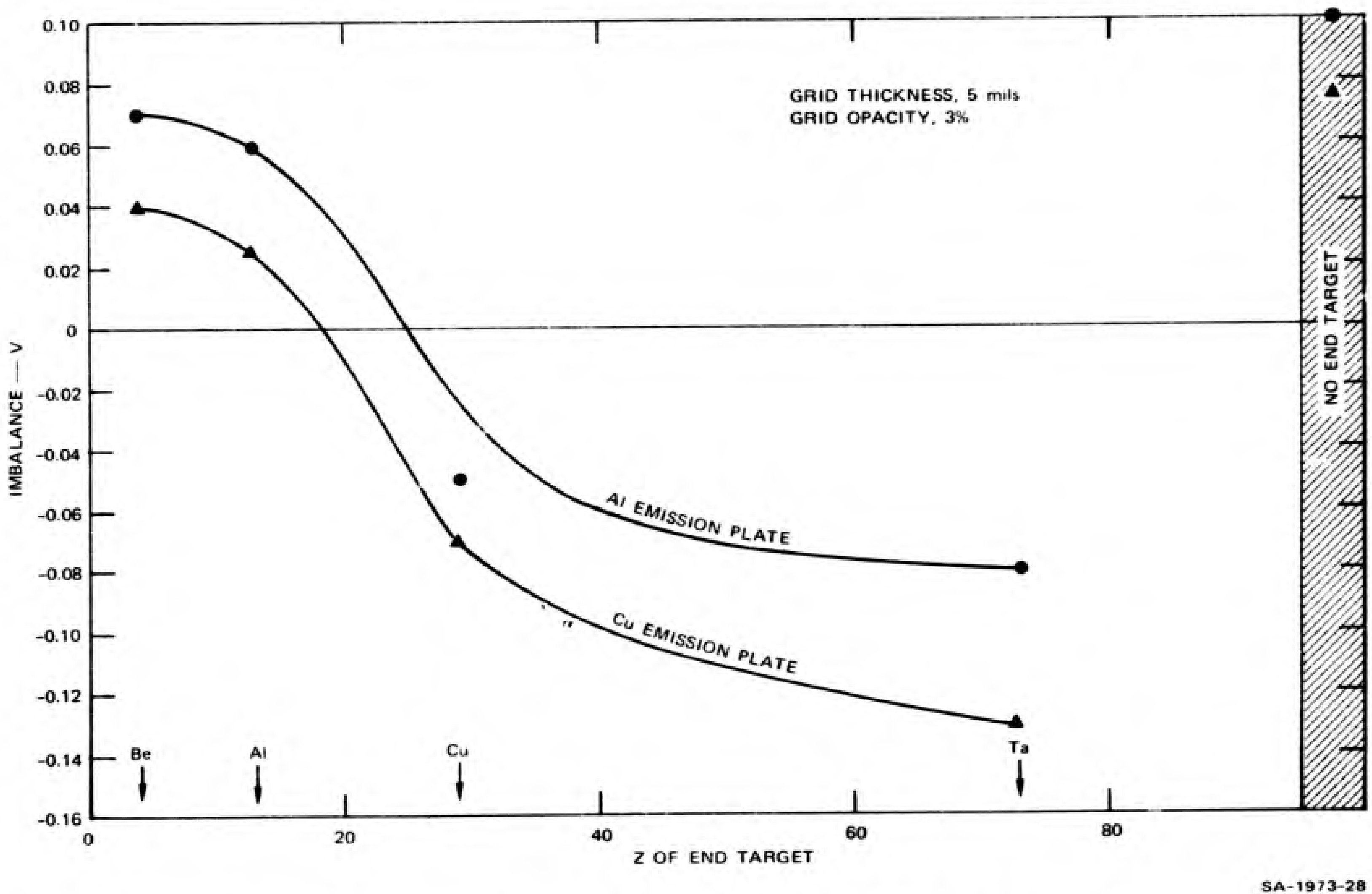


FIGURE 20 IMBALANCE VOLTAGE IN 705 WITH Al GRID, vs. Z OF END TARGET

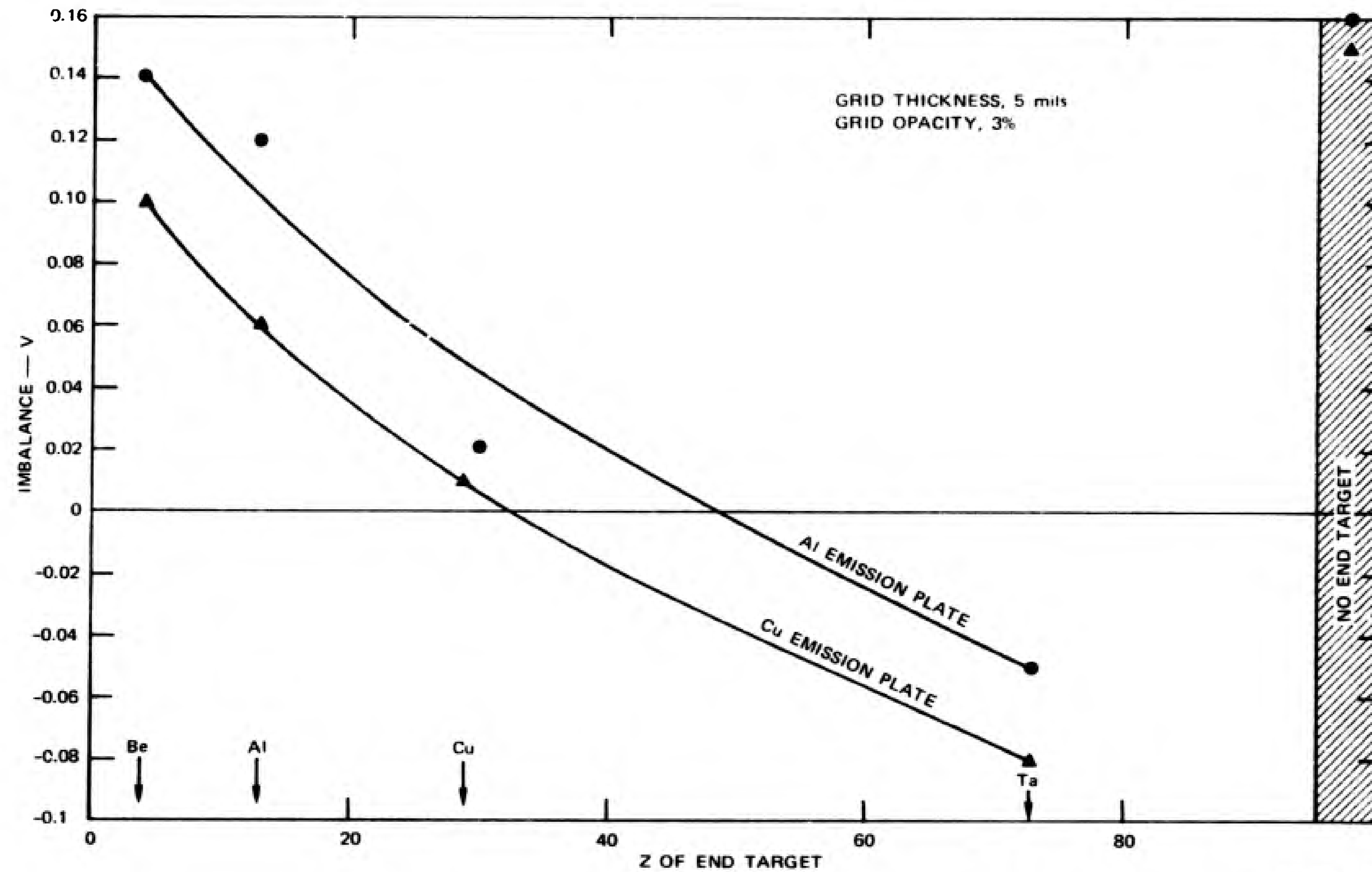


SA-1973-31

FIGURE 21 IMBALANCE VOLTAGE IN 705 WITH Cu GRID, vs. Z OF END TARGET kept in mind that neutralization of the deposited charge is accomplished by collecting electrons if the deposited charge is positive, and by collecting ions if the deposited charge is negative. Since electronic conductivity is several hundred times that of an equal density of ions, an error in the positive imbalance direction would be preferred to a negative imbalance.

## C. Load Circuitry

To make an open-circuit-voltage measurement over an interval of time $\tau$, it is necessary that $RC \gg \tau$, where R is the input impedance of the load circuitry, and C, the capacitance of the grid, is given by

$$C \simeq \epsilon_o A\left(\frac{1}{d_1} + \frac{1}{d_2}\right)$$

where A is the area of the grid, and $d_1$ and $d_2$ are the distances to the cavity end-plates.

If the potential is high enough, one can afford to use passive load circuits such as shown in Figure 22, and accept the voltage division that occurs when a (typically) 50-ohm line is used to transmit the signal to an oscilloscope. From Figure 22(a) it is seen that the voltage will be divided by a factor 50/(R + 50). Since C is usually not greater than about $10^{-11}$ f, even for the 3-ns pulse of the Febetron 706 it is required that $R \gg 300$ ohms, such that the voltage-division factor for the passive system is approximately 50/R. However, when a 100:1 division occurs, few flash X-ray machines have a high enough dose rate (photon mode) to produce potentials (in required volume) that can be detected by the best oscilloscopes. Figure 22(b) shows a capacitive divider circuit that will not load down $C_g$, provided that $R_oC_s \gg \tau$ and $C_c \ll C_g$. For this case, a voltage division of $C_s$:$C_c$ must be acceptable. For very fast pulses or rise times, the circuit in Figure 22(b) can usually be realized in practice better than that of 22(a) because of incidental inductances, etc.

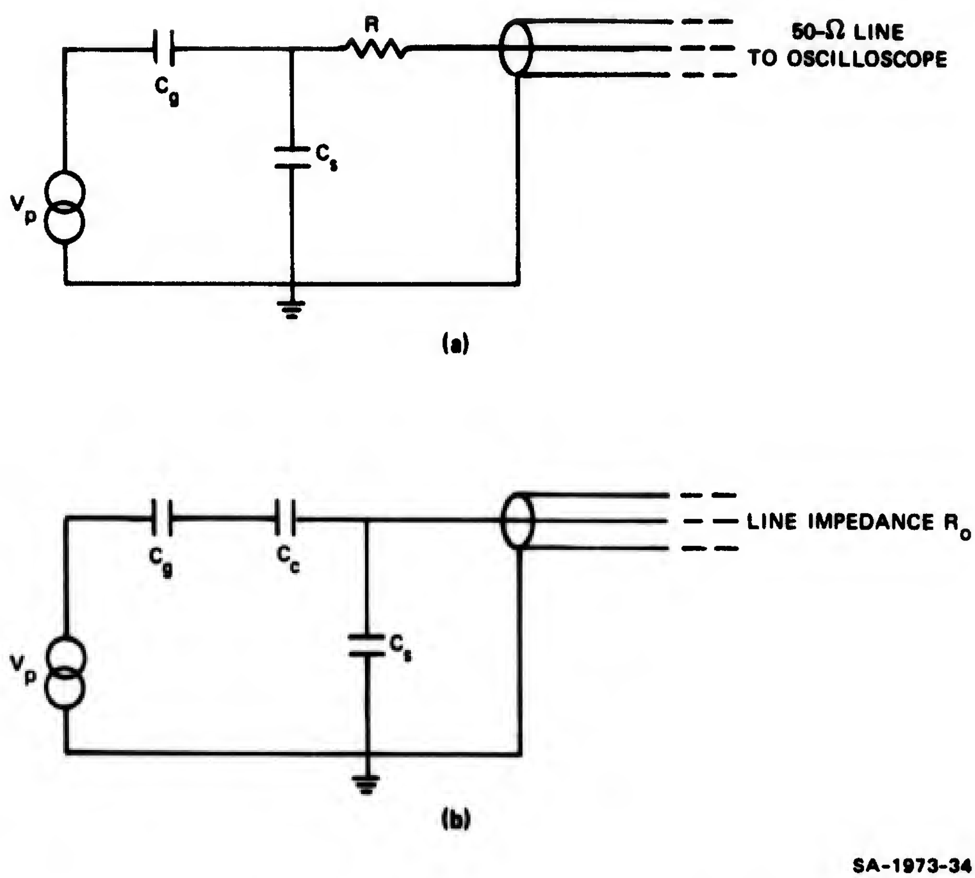


FIGURE 22 CIRCUITS SHOWING LOAD CIRCUITRY FOR PASSIVE LOAD

Thus, the situation often requires amplifiers with a high input impedance and appropriate output impedance to drive the transmission line. Concomitant with this solution, however, is the problem of shielding the amplifier, which is typically more susceptible to TREE effects than are passive elements, particularly solid-state components in the amplifier. Shielding may become a problem even in smaller machines, since often the amplifier must be located near the grid for one or both of the following reasons:

(1) The distance between the amplifier and the grid should be small compared with $c\tau_{min}$.

(2) The incidental shunt capacitance, $C_s$, which also causes voltage division at the output, should usually be kept low.

## D. Aurora Sensor Design

Because of the long duration of Aurora events, it is necessary to have $RC \gtrsim 3 \times 10^{-6}$ s for a good open-circuit measurement. The Aurora beam is quite large, and the rise time is slow, allowing grids to be built with capacitance up to $\sim 10^{-10}$ f (for example, a 30-by-30-cm grid and $d \simeq 1$ cm). However, this capacitance still requires $R \gtrsim 3 \times 10^{4}$ ohms. Even in the region of highest flux the maximum potential is rarely high enough to allow the ~500:1 division that a passive system would require. Thus it is necessary generally to use an amplifier, in which case the input impedance can be made high enough ($10^5$ to $10^7$ ohms) to accommodate the flexibility and/or necessity of smaller grids and also larger d, depending on where the measurement is being made.

Amplifier shielding becomes the major problem in Aurora sensor design. Fortunately, the rise time is long enough that the amplifier can be located at a considerable distance from the grid, allowing the nominal 8 inches of lead thickness required for shielding. Indeed, the rise time of the pulse will allow moving the amplifier from the center of the beam by as much as a meter or two, but other considerations may place an equal or greater restriction on the separation--viz:

(1) The leads may be driven by the Compton currents as a transmission line, resulting in spurious signals generated on the line (another way of looking at the problem of the leads crossing equipotentials).

(2) Incidental shunt capacitance of the leads to the ground may become excessive.

(3) Charge deposition on the leads by direct interaction with incident electrons and photons may become excessive.

All these factors dictate, in addition to keeping the leads short as possible, also keeping the diameter as small as possible, thus maximizing the line impedance in the case of consideration (1), minimizing capacitance in the case of (2), and minimizing the mass in the case of (3). Although it is known that a transmission line with very high impedance has low energy capacity, the total implications of the transmission-line effect (1) are not fully understood at the present time. Measurements shown in Figure C-3 of Appendix C indicate a 100-watt peak power capacity for the 32-mil-diameter, 21-inch-long wire parallel to the Compton current. Certainly, the leads should be placed transverse to the Compton currents to minimize this problem, such that they do not cross equipotential planes. Although charge deposition will be a maximum for this orientation, a fine (3-to-5-mil) wire up to a meter long will have no greater charge deposition than the grids used in Aurora; this deposition was negligible for the 3%-opacity grids. (If the separation, d, is greater than a centimeter, this opacity can be reduced by increasing the wire spacing).

Thus a grid/circuit system for Aurora should consist of a low-atomic-number fine-wire mesh grid with total area as small as $10^{-2}$ $m^2$, with opacity of 3% or less. Fine wires (less than 1 meter long and 3 to 5 mils in diameter) placed as remote from "ground" as possible should lead to an amplifier with an input impedance greater than $10^5$ ohms, and output impedance to match the cables leading to the data room. The shunt capacitance of the wire leads between the grid and amplifier should be measured so that the voltage division can be determined. The leads should be oriented transverse to the Compton currents so that they remain in equipotential planes as much as possible. The amplifier should be shielded from TREE effects, needing as much as an 8-inch thickness of lead near the high-flux region.

# VII DISCUSSION AND RECOMMENDATIONS FOR FUTURE WORK

## A. Prospects for Low-Impedance Techniques

The work described in this report has been aimed principally at the technique of measuring potentials and difference of potentials using the near-open-circuit technique--i.e., in measuring, using so little energy stored in the sensor that the measuring process has a negligible effect on the sensor's potential. Furthermore, we have examined the perturbation, by the sensor, of the potential in the plane where it is placed; this perturbation occurs largely through charge deposition on the sensor. We have demonstrated a method of correcting for the charge deposition by noting that it accumulates on the grid during the pulse and persists afterward, unless low-energy high-density plasma action resists the accumulation. This opposition to the charge accumulation occurs naturally in a plasma, since charge on the grid will cause it to have a potential different from its plasma/field environs, and plasmas resist the existence of electric fields by the mechanism of current flowing to oppose the fields. Thus, even though a plasma with high enough conductivity ruins the ability to measure the error signal, it also tends to remove the error, which is a preferred result for any measurement except perhaps one intended as a parametric study of such errors.

It is important to note the difference between the short-pulse machines and Aurora so far as the negative and positive ions are concerned. It is noted in Appendix A that for times long compared with the attachment time and short compared with recombination times, both of these accumulate approximately proportionally to the time squared. In the Febetron 705, even though the electron density may reach a peak of $10^{11}$ el/cm$^3$, the density of positive and negative ions is not very significant. Although the positive and negative ions accumulate without much decay because recombination is so slow, the pulse lasts only 50 to 60 ns. In Aurora, with similar dose rates, the peak electron density reaches less than an order of magnitude higher than in the 705 and decays soon after the pulse. Hence, during a long-duration pulse, the positive-ion conductivity can act significantly to oppose electron accumulation on a grid. Then, following the pulse, after the electrons have attached out, negative ions as well can be effective in neutralizing any residual charges.

The above discussion is appropriate to lead into a discussion of low-impedance techniques for diagnosing the complex field/environment system produced by both flash X-ray machines and nuclear detonations. The difficulty with low-impedance techniques is the need to interpret the measured quantity in view of the interaction between the sensor and the system it is diagnosing. For example, when a grid or stub connected to an impedance Z is placed in a space-charge field, its potential will generally ride somewhere between ground and the local potential, $V_p$ (neglecting charge-deposition effects). Taking the usual case when the space-charge is negative, the sensor will then attract an electron current $I_e$, and the potential of the sensor will be

$$V = I_e Z \ . \qquad (1)$$

Now, in its simplest form we can express $I_e$ by

$$I_e = (V_p - V)/R_\sigma \qquad (2)$$

where $R_\sigma$ is the composite resistance of the plasma between the sensor and the nearby space charge of potential $V_p$. Combining Eqs. (1) and (2) gives the sensor potential

$$V = V_p/(1 + \frac{R_\sigma}{Z}) \qquad (3)$$

which shows that $V \simeq V_p$ only when $Z >> R_\sigma$. Thus a low-impedance measurement of potential can be simply interpreted, provided that the plasma conductivity and current-collecting ability of the sensor combine to give $R_\sigma << Z$. That such a low plasma resistance is difficult to achieve is attested by the apparent failure of low-impedance techniques in Aurora despite the relatively high conductivity in the high-dose region (see Appendix C). The results of Figures C-2(a) and C-2(b) seem to indicate that the Aurora grids collect enough current even when connected to 50-ohm line, to attain about half the open-circuit measured results. However, the differential measurements of Figures C-2(c) and C-2(d), when higher impedance was used, seem to obscure rather than confirm this conclusion. It is conceivable, however, that large grids used in situations with higher-conductivity plasmas (e.g., at low pressure but very high electron density) would allow this simple interpretation.

Short of this, the space-charge potential could still be inferred from Eq. (3), but considerable additional analysis and/or diagnostics would be required to evaluate $R_\sigma$.

## B. Transmission-Line Measurements

An adjunct to the Aurora sensor tests was measurement of signals induced in transmission lines in the large Aurora test cell, exterior to the cassette used for sensor measurements. These tests were part of a preliminary study sponsored jointly by Air Force Weapons Laboratory and DNA.[9] Some measurements in the cassette as well as the test cell are related to the question of coupling of a longitudinal field to wires immersed in a medium with time-varying conductivity. For example, transmission lines, as in the deposition region of a nuclear burst. In addition to the suitability of the Aurora facility, the development of the electric-potential and -field sensors for this facility offers an important tool necessary in the interpretation of the measurements for this facility.

The close-in and intermediate-range coupling to power lines and other conductors leading to strategic and communication facilities is not understood at this time. An important complicating factor is the time-varying conductivity of the air surrounding the conductors. In attempting to understand transmission lines in this geometry, it is instructive to first consider the close-in and intermediate-zone phenomena without the line present. Briefly, the conducting air and earth act as paths for "return" current, completing a circuit that begins with the Compton currents as a source. The addition of a transmission line parallel to the Compton currents will add another path for return currents, perturbing the basic local field/environment system. Note that the effects of such a line differ considerably from the effects of a grid in an equipotential plane, in that the line "shorts out" the field, crossing what would be equipotentials and providing the extra return path which is punctuated by periodic "risers" between ground and line.

It is recommended that a program be undertaken consisting of comprehensive testing of various model geometries in the Aurora test cell, accompanied by an analytical effort to predict both the test configurations exposed to the Aurora environment and the more complex full-scale-facility lines exposed to the nuclear environment.

It appears that the Aurora beam-produced field/environment system has an unexpected characteristic that enhances its worth in simulating phenomena associated with low-altitude and surface bursts. This characteristic is what might be called late-time effects, which in Aurora refers to the persistence of the fields after the photon pulse is ended. Since the conductivity of the enveloping plasma is quite different in the period following the pulse than it is during the pulse, the response of transmission lines will be quite different during the two periods even though the driving fields may be comparable. A program for testing transmission lines in Aurora should take advantage of this added nuclear-burst-related phenomenon, although considerable analysis and/or diagnostic measurements may be required to sufficiently understand the nature of Aurora's late-time effects.

## REFERENCES


1. G. K. Schlegel, private communication.

2. A. L. Whitson, private communication.

3. A. L. Whitson, private communication.

4. S. I. Taimuty, R. H. Stehle, and A. L. Whitson, "A Laboratory Study of Radiation Effects on E-field Sensors," Final Report, Contract F29601-69-C-0107, SRI Project 7974, Stanford Research Institute, Menlo Park, Calif. (November 1970).

5. Aurora Facility Brochure, Harry Diamond Laboratories, Washington D. C. (September 1972).

6. C. E. Baum, "Radiation and Conductivity Constraints on the Design of a Dipole Electric Field Sensor," Note 15, Electromagnetic Pulse Sensor and Simulation Notes, AFWL EMP 1-1, Air Force Weapons Laboratory, Albuquerque, N. M. (June 1970).

7. C. E. Baum, "A Technique for Measuring Electric Fields Associated with Internal EMP," Note 24, Electromagnetic Pulse Sensor and Simulation Notes, AFWL EMP 1-1, Air Force Weapons Laboratory, Albuquerque, N. M. (June 1970).

8. Lt. Larry Williams, private communication.

9. W. C. Taylor and K. A. Graf, "Measurements of Electric Field Coupling in a Radiation Environment," Technical Memorandum 23, Contract F29601-69-C-0127, SRI Project 7995, Stanford Research Institute, Menlo Park, Calif. (October 1973).

## Appendix A

## ESTIMATES OF POTENTIALS AND FIELDS

### 1. Electron and Ion Concentrations

The photon pulses of the three machines used in this program have a leading edge nearly enough linear that a linearly increasing dose rate was used in analyzing the events occurring during the first portion of the pulses. In air, the ionization rate is given by

$$S = C_e \dot{\gamma} \frac{\text{ionizations}}{m^3 - s} \tag{A-1}$$

where $C_e = 2.1 \times 10^{15}$ and $\dot{\gamma}$ is the dose rate in rad/s. For $\dot{\gamma}$ linear with time, $\ddot{\gamma}$ is a constant, giving $S = Ct$ for the leading edge, where $C \equiv C_e \ddot{\gamma}$. To evaluate the conductivity for a pulse as long as Aurora's, it is necessary to determine the concentration of positive ions, $n_+$, and negative ions, $n_-$, as well as the electron density, $n_e$. The differential equations that determine the temporal character of these densities are

$$\frac{dn_e}{dt} = S - \beta n_e - \alpha n_+ n_e \tag{A-2}$$

$$\frac{dn_+}{dt} = S - \alpha n_+ n_e - \gamma n_+ n_- \tag{A-3}$$

$$\frac{dn_-}{dt} = \beta n_e - \gamma n_+ n_- \tag{A-4}$$

where $\beta$ is the attachment frequency, $\alpha$ is the electron-ion recombination coefficient and $\gamma$ is the ion-ion recombination coefficient. For our estimates, we use the values

$$\beta = 10^8 \ s^{-1}$$

$$\alpha = 4.5 \times 10^{-12} \ m^3/s$$

$$\gamma = 2.3 \times 10^{-12}\ m^3/s.$$

It can be shown that because of the low values of $\alpha$ and $\gamma$, for all dose rates of interest, the recombination terms in the differential equations can be ignored for the first 80 ns, the approximate duration of the Aurora pulse leading edge. This gives a simplified set:

$$\frac{dn_e}{dt} \simeq Ct - \beta n_e \tag{A-5}$$

$$\frac{dn_+}{dt} \simeq Ct \tag{A-6}$$

$$\frac{dn_-}{dt} \simeq \beta n_e \quad . \tag{A-7}$$

Solution of these gives

$$n_e \simeq (C/\beta^2)\ [\beta t - (1 - e^{-\beta t})] \tag{A-8}$$

$$n_+ \simeq \tfrac{1}{2} Ct^2 \tag{A-9}$$

$$n_- = n_+ - n_e \quad . \tag{A-10}$$

These concentrations, normalized by $C = C_e\dot{\gamma}$, are graphed in Figure A-1. It is concluded that the electrons will dominate the air conductivity for times up to 100 ns. Since their mobility, $\mu$, is much higher than that of ions, this will more than compensate for the lower concentration shown in Figure A-1.

## 2. Generation of Electric Fields--Free-Field Case

From Maxwell's equation

$$\nabla \times \vec{H} = \vec{J} + \epsilon \frac{\partial \vec{E}}{\partial t} \tag{A-11}$$

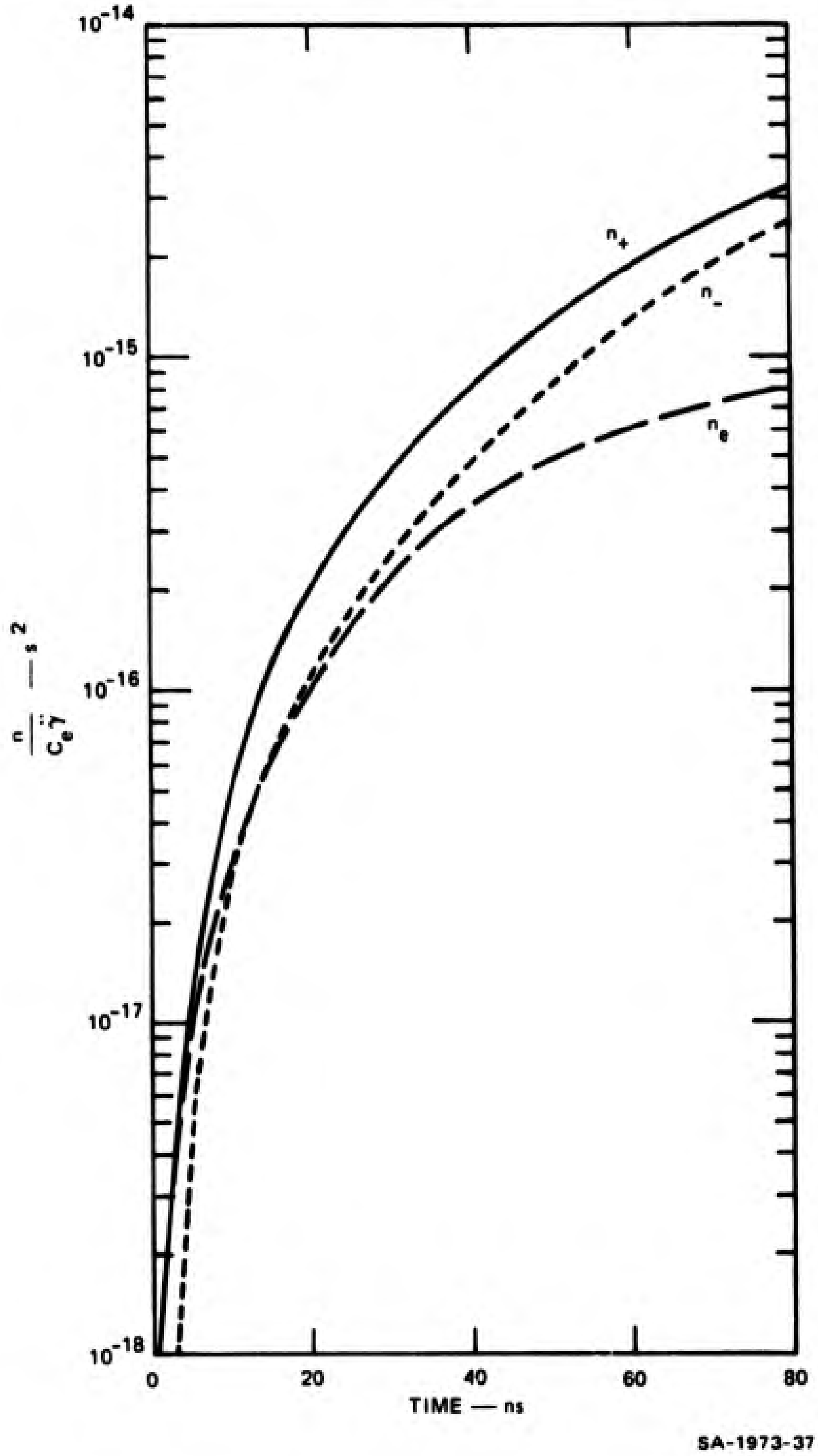


FIGURE A-1 NORMALIZED ELECTRON AND ION DENSITIES vs. TIME FOR A LINEARLY-INCREASING DOSE RATE (one atmosphere) we simplify by considering $\vec{J}$ and $\vec{E}$ limited to a single direction and uniform transverse to this direction, giving $\nabla \times \vec{H} = 0$. The current density J is comprised of two components: (1) $J_D$, the current source of driving electrons (Compton and photoelectric), which are sufficiently energetic that the generated fields do not affect their motion, and (2) the low-energy plasma or conduction electron current, given by $J_\sigma = \sigma E$, which will flow opposite the source currents. Thus the electric field, from Eq. (A-11), is determined by

$$\epsilon \frac{\partial E}{\partial t} = -J_D - \sigma E \quad . \tag{A-12}$$

For the high collision frequency at one atmosphere, the transient air conductivity is equivalent to dc conductivity, $\sigma = n_e e\mu$, for all times of interest. Also, there is no significant time lag or out-of-phase component of $\sigma$ such as that which is sometimes included in the dielectric constant for sinusoidally varying field, allowing us to set $\epsilon = \epsilon_o$. Using $\mu$ independent of E and t, Eq. (A-12) becomes

$$\epsilon_o \frac{\partial E}{\partial t} = -J_D - n_e(t)e\mu E \quad . \tag{A-13}$$

This analysis is limited to sufficiently low potentials that the electrons compromising $J_D$ are unaffected by the generated potentials. (Such a limitation is reasonable for all the measurements reported here.) Hence, $J_D$ is independent of E in Eq. (A-13). Another means by which $J_D$ could be a function of E arises when the air offers a finite conductivity, $\sigma_D$, to the source electrons. For this case, expressing Ohm's law for both currents gives $J_D = \sigma_D E_D$ and $J_\sigma = \sigma E_\sigma$, where the resulting, or total, field E consists of $E_D + E_\sigma$. However, for high-energy driving electrons, $\sigma_D$ is usually so high that $E_D << E_\sigma$, and Eq. (A-13) is a good approximation with $J_D$ independent of E.

Because of the complicated form of $n_e(t)$ from Eq. (A-8), we consider two simplified regimes in time. First, for $t \lesssim \beta^{-1}$, it can be seen from Eq. (A-8) that

$$n_e \approx \tfrac{1}{2} C t^2 \quad . \tag{A-14}$$

Substituting into (A-13) and solving for E gives

$$E(t) = -\left(\dot{J}_D \tau_1^{\,2}/\epsilon_o\right)\left[e^{-t^3/\tau_1^{\,3}} \int_0^{t/\tau_1} s\, e^{s^3}\, ds\right] \tag{A-15}$$

where

$$\tau_1 \equiv (6\, \epsilon_o / e\mu\, C)^{1/3} \quad . \tag{A-16}$$

It will be seen that $\tau_1$ is often less than $\beta^{-1}$, so that we need to consider times from less than $\tau_1$ to much greater than $\tau_1$. Again, simplifying by asymptotic approximation in time, we get:

$$E(t) = -J_D\, t^2/2\epsilon_o \qquad \text{for } t \ll \tau_1 \tag{A-17}$$

and

$$E(t) = -J_D\, \tau_1^{\,3}/3\epsilon_o t \qquad \text{for } t \gg \tau_1 \tag{A-18}$$

$$\left.\begin{matrix} t \ll \tau_1 \\ t \gg \tau_1 \end{matrix}\right\} t \lesssim \beta^{-1} \text{ (high-flux case)} .$$

The second simplified approximations are for $t \gg \beta^{-1}$ (applicable to Aurora only), giving $n_e(t) \simeq Ct/\beta$, and from Eq. (A-13),

$$E(t) = -\left(J_D \tau_2^{\,2}/\epsilon_o\right) e^{-t^2/\tau_2^{\,2}} \int_0^{t/\tau_2} s\, e^{s^2}\, ds \tag{A-19}$$

where

$$\tau_2 \equiv (2\, \beta\, \epsilon_o / e\, \dot{\mu}\, C)^{\frac{1}{2}} \quad . \tag{A-20}$$

The same two approximations in time give

$$\left.\begin{array}{lll} E(t) = -\dot{J}_D\, t^2/2\epsilon_o & \text{for } t \ll \tau_2 & \text{(A-21)} \\ & \text{(low-flux case)} & \\ \text{and} & & \\ E(t) = -\dot{J}_D\, \tau_2^{\,2}/2\epsilon_o & \text{for } t \gg \tau_2 & \text{(A-22)} \end{array}\right\} \quad t \gg \beta^{-1} .$$

In addition to the asymptotic limits of Eqs. (A-15) and (A-19), we have determined the maximum value of E(t) and the time at which it occurs, for application to the Febetron 705 and Aurora tests. Thus, in Eq. (A-15) the term in brackets has a maximum value of approximately 0.30 at $t = 1.1\ \tau_1$, giving

$$E_{max}(1.1\ \tau_1) = -0.30\ \dot{J}_D\ \tau_1^{\,2}/\epsilon_o\ , \qquad t \lesssim \beta^{-1}\ . \tag{A-23}$$

However, this estimate is valid only if $E_{max}\ (1.1\ \tau_1)$ is much greater than the limit given for large times by Eq. (22)--i.e., when

$$0.30\ \tau_1^{\,2} > 0.5\ \tau_2^{\,2} \tag{A-24}$$

which reduces to

$$\beta\tau_1 < 1.8. \tag{A-25}$$

This condition gives the result

$$t(E_{max}) < 2\beta^{-1}. \tag{A-26}$$

Thus we may define the low-flux case as that for which the neutralization time is long compared to the attachment time $\beta^{-1}$; the field reaches a weak maximum before decreasing to an asymptotic limit at $t \gg \beta^{-1}$. The high-flux case is that for which the neutralization time is short compared to $\beta^{-1}$. Then the field has a maximum before $t = 2\beta^{-1}$ and subsequently decreases to an asymptotic limit at $t \gg \beta^{-1}$.

In terms of previous definitions, the high-flux case is established when

$$\ddot{\gamma} > \beta^3 \epsilon_o / e\mu C_e \qquad \text{rad/s}^2 \quad . \tag{A-27}$$

If we approximate $\ddot{\gamma}$ by $\dot{\gamma}_p / t_p$, where the subscript p refers to the time of peak radiation flux, then the high-flux case is

$$\dot{\gamma}_p > t_p \, \beta^3 \, \epsilon_o / e\mu C_e \quad . \tag{A-28}$$

Using $t_p = 80$ ns and $\overline{1/\mu} = 3.5$ (high field), for Aurora we have

$$\dot{\gamma}_p > 7.4 \times 10^9 \text{ rad/s} \quad . \tag{A-29}$$

For the Febetron 705, we use $t_p = 16$ ns and $\overline{1/\mu} = 2$ (low field), giving

$$\dot{\gamma}_p > 8.4 \times 10^8 \text{ rad/s} \quad . \tag{A-30}$$

Both machines are capable of exceeding these criteria in their high-dose target zones.

It is noted that the above theory is for an unbounded region of space. Although the Aurora test cell is large, the pulse duration is sufficiently long that the effects of currents induced in the conducting walls by the beam currents will probably modify the fields calculated in this appendix. However, no calculations or estimates of this perturbation have been made.

### 3. Fields Between Parallel Plates

Taking the divergence of each term in Eq. (A-13) gives

$$\varepsilon_o \operatorname{div} \dot{E} = \dot{q}_D - \operatorname{div}(ne\mu E) \qquad \text{(A-31)}$$

where $q_D$ is the charge density of the source electron flux, obeying the relationship $\dot{q}_D = -\operatorname{div} J_D$. Integrating Eq. (A-31) over the space between parallel plates located at x = 0 and d, and applying boundary conditions that $\dot{E}(d/2) = J(d/2) = 0$, we get

$$\varepsilon_o \dot{E} = \dot{q}_D\ (x - d/2) - ne\mu E \qquad \text{(A-32)}$$

assuming that $\mu$ is constant in both space and time and that $\dot{q}_D$ is not attenuated significantly in traversing the cavity.

Treating the early-time case, we substitute Eq. (A-14) into (A-32) and integrate over t, giving

$$E(t) = (\tau_1/\varepsilon_o)\ \dot{q}_D(x - D/2)\ F(t/\tau_1) \qquad \text{(A-33)}$$

where

$$F(y) = e^{-y^3} \int_0^y e^{s^3}\, ds$$

for which F(0) = 0 and F(y) has a maximum at F(0.8) = 0.55. Substitution of the various machine parameters shows that the minimum value of $\tau_1$ is about 6 ns, indicating that neutralization can occur according to Eq. (A-33) in the Febetron 705 and in Aurora, but will be too slow for the short Febetron 706 pulse.

## Appendix B

## ANALYSIS OF SENSOR RESPONSE

### 1. General

It is assumed that a grid is located in an equipotential plane between parallel plates, as shown in Figure 5. The shift in grid potential due to charge deposition can be expressed simply when charge imbalance results from grid-to-wall or wall-to-grid charge transport. This is the case in vacuum under non-space-charge-limited conditions (small potentials compared to electron energies), and at pressures where the emissions and stopping power of air do not modify the charge transport. The uncharged grid floats at the environmental potential $V_p$; however, the photon and electron interactions are operative during the radiation pulse. After a surface-charge density $Q_g$ has collected on the grid, the new potential V is given by

$$C_g(V - V_p) = Q_g \tag{B-1}$$

where $C_g$ is the grid capacitance to ground (walls). We have also assumed that the grid does not significantly alter the space-charge distribution in the cavity--e.g., by substantial absorption of the Compton current or by emission of large electron fluxes.

A description of the mechanisms that contribute to charge imbalance is required for the design of sensors and interpretation of measurements. We consider here the deposition of charge on the grid by the following mechanisms:

(1) Emission of electrons from the grid by interactions with the incident photon flux (Compton electron and photoelectron production).

(2) Absorption by the grid, of electrons from the incident Compton and photoelectric fluxes.

(3) Collection (when air is present) of conduction current resulting from the air ionization and electric field at the grid surface.

(4) Current drawn from the grid due to the finite impedance of the voltage probe used to measure the grid potential.

When plasma is present, the floating potential of the grid will also be shifted by collection of random thermal electrons. However, this effect is generally small compared to the potentials of interest and will not be considered. The net collected surface-charge density on the grid $Q_g$ will be the algebraic sum of the contributions of the above four mechanisms represented by $Q_\gamma$, $Q_e$, $Q_c$, $Q_z$, respectively. Similar subscripts will be used to represent their time derivatives.

We differentiate the charge-balance, Eq. (B-1), to more readily display the imbalance currents:

$$C_g(\dot{V} - \dot{V}_p) = I_\gamma + I_e + I_c + I_z \ . \tag{B-2}$$

2. Photoemission and Absorption of Electrons by the Grid

The amount of emission and absorption by the grid in the environmental fluxes is characterized by the incident spectra and the intrinsic photon/electron response functions of the grid. A particular grid will have a characteristic response function that is dependent on the atomic number, density, thickness, and transparency of the grid. The response functions are also dependent on the photon/electron energy and incident angle. In general, when the response function and the incident spectrum are known, the balance current can be obtained from an integral over energy and angle of the product of these two quantities. It was considered beyond the scope of this program to make quantitative predictions of $I_\gamma$ and $I_e$.

There are two means for the plasma to contribute charge to the grid proper. The simplest one to evaluate is the physical interception of the neutralizing current by the grid, assuming there is no charge on the grid due to other sources. If the electric field at the sensor position is E and the conductivity is $\sigma$, then the plasma current will be $\sigma E$. The fraction of this current intercepted by the grid depends on the physical cross section, a, of the grid, giving

$$I_i = -a\sigma|E| \tag{B-3}$$

where the absolute value is used because the grid collects electrons but does not emit them readily. The current collected by this mechanism is not expected to shift the potential significantly, provided that the grid has a high transparency factor A/a.

However, the second mechanism for plasma-current collection by the grid may be more significant. It will occur when (because of one of the other imbalance sources) the difference in potential between the local space charge and the grid causes the grid to behave as a probe in the plasma, so that it draws current. This effect, too, is asymmetrical since the electrons can move more efficiently to the grid (as occurs when the grid has a positive imbalance) than ions can (as occurs when the grid has a negative imbalance). Thus, for experiments at high pressures, such as one atmosphere, the current collected by the grid will be given by

$$I_{probe} = -a'\sigma|E_g| \tag{B-4}$$

where $E_g$ is the local field at the grid due to the imbalance charge on it, and $a'$ is an effective area of the grid, higher than the projected area a, because the individual grid wires generally draw current from all directions when the grid acts as a probe. The field $E_g$ will be related to the voltage difference, $V - V_p$, by

$$|E_g = |V - V_p|/d_{eff} \qquad \text{(B-5)}$$

where $d_{eff}$ is an effective distance over which the charged grid is perturbing the space-charge potential. Then

$$I_{probe} = - |V - V_p|/R_\sigma$$

where $R_\sigma = d_{eff}/a'\sigma(t)$. Thus, $I_c$ is the sum of $I_i$ and $I_{probe}$, both of which, for practical purposes, consist only of electron collection by the grid, but by different mechanisms. For only high-transparency grids, we consider $I_i$ negligible compared with $I_{probe}$, giving

$$I_c \simeq - |V - V_p|/R_\sigma \ . \qquad \text{(B-6)}$$

Since $I_c$ tends to counter any positive imbalance voltage, it actually represents a mechanism for partial alleviation of the imbalance problem of that polarity. Because of low dose rate and short pulse duration, effects of $\sigma(t)$ are not seen in the Febetron 706. However, alleviation effects may be present in the 705 tests, especially during the last half of the pulse, when the conductivity is highest, and it will be seen that this alleviation is a major factor in the Aurora measurements.

3. Imbalance by Circuit Loading

The voltage-probe circuit attached to the grid can also cause a charge buildup, resulting in a shift of grid potential. We consider here the effect of probe resistance R and shunt capacitance $C_s$. The imbalance current $I_z$ is the sum of the currents through R and $C_s$, so

$$I_z = -(V/R + C_s\dot{V}) \quad . \tag{B-7}$$

As is usual in probe applications, large resistance and small shunt capacitance are desirable.

## 4. Description of Sensor Response to Charge-Imbalance Mechanism

The air-conduction and circuit-loading currents are now explicitly included in the charge-balance equation:

$$C_g(\dot{V} - \dot{V}_p) = I_\gamma + I_e - |V-V_p|/R_\sigma - (C_s\dot{V} + V/R) \quad . \tag{B-8}$$

This equation can be rearranged into a more convenient form for the description of an electrical lumped-circuit analog useful in modeling sensor response:

$$\dot{V} + \frac{V}{R(C_g + C_s)} = \frac{C_g}{C_g + C_s}\dot{V}_p + \frac{(I_\gamma + I_e)}{(C_g + C_s)} - \frac{|V - V_p|}{(C_g + C_s)R_\sigma} \quad . \tag{B-9}$$

The analog circuit is shown in Figure 6, where $\dot{V}_p$ is represented by a zero-impedance voltage source dirving the grid to potential V through the grid capacitance $C_g$. The photon- and electron-imbalance currents are represented by an infinite-impedance current source I. This current source is referenced to ground only when the electron ranges are long compared with the grid separation from the plates. The path for plasma (electron) current collection at the grid is represented approximately by the resistance $R_\sigma$ and diode. The much smaller ion current may be thought of as flowing against the reverse impedance of the diode. Although this electrical analog applies to the IEMP case, a circuit for other environments, such as the EMP case, will differ somewhat.[6]

In the analog circuit the capacitance $C_g$ represents the coupling of space charge to the grid during the pulse. Following the space-charge pulse, $C_g$ becomes the grid-to-ground capacitance, and the circuit shown in Figure 6 has the same form as during the pulse, since $V_p$ goes to zero while the voltage-source impedance remains zero. The electrical analog circuit allows visualization of the sensor interaction, and is useful in modeling sensor responses to arbitrary environmental potentials and imbalance currents, providing an approximate electrical solution of Eq. (B-9).

5. Interpretation of Experimental Sensor Data

In addition to predicting sensor response for design purposes, it is necessary to interpret the results of the flash X-ray tests in terms of the effects of charge imbalance. A method for experimentally discriminating between the space-charge potential and the charge-imbalance effect has been established. It depends on the persistence of the collected charge on the grid after the space-charge pulse has passes. When $V_p = 0$ and $R(C_g + C_s) >> \tau$, the residual sensor potential after a pulse of duration $\tau$ is

$$V(\tau) = \int_0^\tau dt \left[ \frac{I(t) - |V - V_p|/R_\sigma(t)}{C_g + C_s} \right] . \tag{B-10}$$

That is,

$$Q_g(\tau) = (C_g + C_s)\, V(\tau) . \tag{B-11}$$

Since the neutralizing currents are at work during the pulse, we must also impose the restriction $\epsilon_o/\sigma >> \tau$, to obtain an accurate value of $Q_g$.

It is possible to determine the value of $V_p(t)$ without measuring the imbalance currents, when their time dependence is known. This is generally the case when only $I_\gamma$ and $I_e$ contribute to charge imbalance.

The imbalance current I(t) then has essentially the same time dependence as the primary photon/electron flux, which is recorded by the photon detector. If the imbalance current is Kf(t), where f(t) is known, then

$$V(\tau) = \frac{K}{C}\int_0^{\tau} f(t)dt \tag{B-12}$$

and

$$V_p(t) = V(t) - V(\tau)\left[\int_0^{t} f(t)dt\right] / \left[\int_0^{\tau} f(t)dt\right] \tag{B-13}$$

which has the merit of describing the desired potential as a function of time in terms of measurable quantities.

A convenient special case arises if f(t) is symmetrical about the peak, as is approximately true of the Febetrons and Aurora (in the absence of air ionization). Then the ratio of the two integrals in Eq. (B-13) is ½ at the peak ($t = \tau/2$), resulting in

$$V_p(\tau/2) = V(\tau/2) - \tfrac{1}{2} V_{bal}(\tau) \tag{B-14}$$

which gives a very simple determination of the peak space-charge potential when charge imbalance due to $I_\gamma$ and $I_e$ is present.

## Appendix C

### AURORA LOW-IMPEDANCE MEASUREMENTS

In addition to the open-circuit-voltage measurements described in Section V-C, some low-impedance measurements were also made in the Aurora double cassette. These tests were made (1) for comparison with the open-circuit results, (2) to determine if there is a feasible low-impedance technique without active electronics for use in the radiation environment, and (3) to measure coupling of the longitudinal electrical field to wires in the radiation-induced plasma.

Figure C-1 is a comparison of open-circuit measurements on the grids in one cubicle assembly without an end-plate, versus the signal from a 2.3-inch-long monopole mounted perpendicular to the emission plate (as a ground plane) in another "cubicle." The monopole was actually made of 6 parallel wires, each 32-mils in diameter, on a circle 2 cm in diameter. This forms a "fatter" monopole while presenting a low cross section for interaction with photons and electrons. The open-circuit potential of the monopole [Figure C-1(a)] reaches a maximum of about 40 volts, which is rather consistent with the 70-volt grid 4 inches from the emission plate. Figure C-1(b) shows that connecting the dipole directly to the 50-ohm line loads the voltage down to about a 15-volt peak, although the pulse shape is quite similar to the open-circuit pulse.

Figure C-2 shows measurements with grids connected to low-impedance circuits, for comparison with the open-circuit potentials of Figure C-1(c) and C-1(d), which reached maximums of about 70 and 90 volts, respectively. The two grids connected directly to 50-ohm cables gave about 35 volts (4-inch spacing) and 40 volts (7-inch spacing). Using a balun transformer with balanced 600-ohm input to difference the grid



Preceding page blank

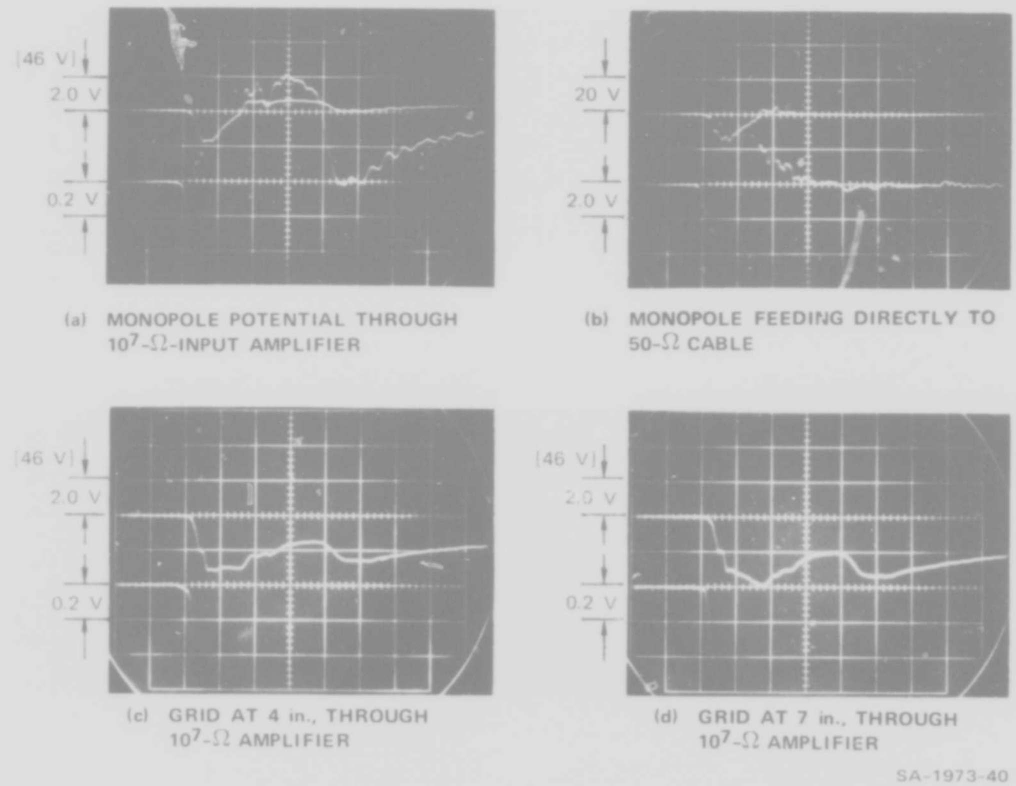


FIGURE C-1 COMPARISON OF MONOPOLE MEASUREMENTS WITH GRIDS

signals, the maximum difference was 3 to 4 volts. The transformer was located in the lower cassette compartment. Another differentiating measurement on the same grids employed 78-ohm twinax cable leading to a transformer in the data room. This measurement gave a maximum difference of 7 to 8 volts, and the pulse shape was different from the 600-ohm measurement. Neither measurement comes very close to the 20-volt difference between the open-circuit potentials.

Finally, Figure C-3 shows measurements of voltages developed across loads connected at two ends of a 21-inch long 32-mil-diameter aluminum wire in the grid compartment, running parallel to the Compton currents and 6 inches above the lead-brick ground plane. The

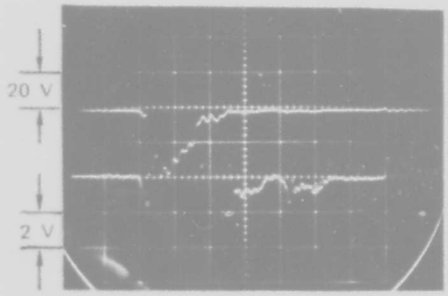


(a) GRID AT 4-in. POSITION, FEEDING DIRECTLY TO 50-Ω CABLE

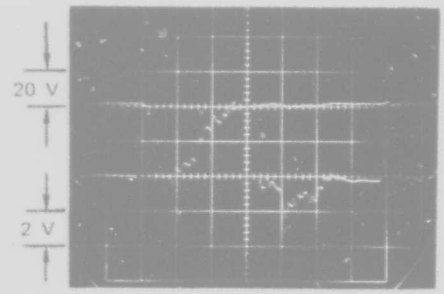


(b) GRID AT 7-in. POSITION, FEEDING DIRECTLY TO 50-Ω CABLE

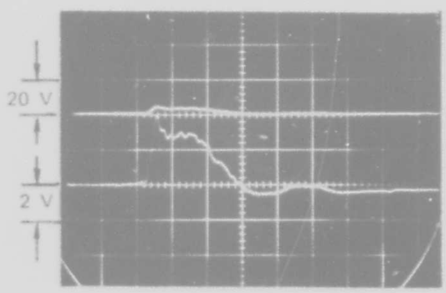


(c) GRIDS AT 4 in. AND 7 in., DIFFERENCED THROUGH 600-Ω BALUN

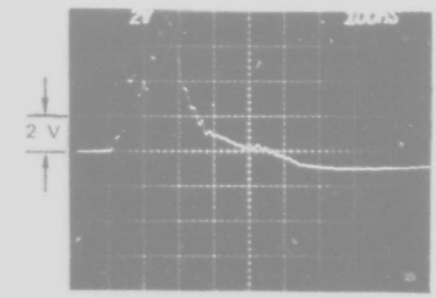


(d) GRIDS AT 4 in. AND 7 in., DIFFERENCED THROUGH 78-Ω TWINAX CABLE

SA-1973-43

FIGURE C-2 MEASUREMENTS WITH GRIDS CONNECTED TO LOW-IMPEDANCE CIRCUITRY

loads were 5, 50, and 520 ohms. It is seen that for most of the pulse the currents were induced in a direction opposite to the Compton currents for the two low-impedance loads. The higher current at the source end is reasonable in view of the higher plasma conductivity ($\sim 5 \times 10^{-2}$ mhos/m) at that end. Since the plasma is part of the conducting system, currents flow between the wire and ground through the plasma. The negative voltages on both ends with the 520-ohm termination indicate that the line impedance is lower than 520 ohms.

A detailed investigation of these low-impedance results was not considered within the scope of this project.

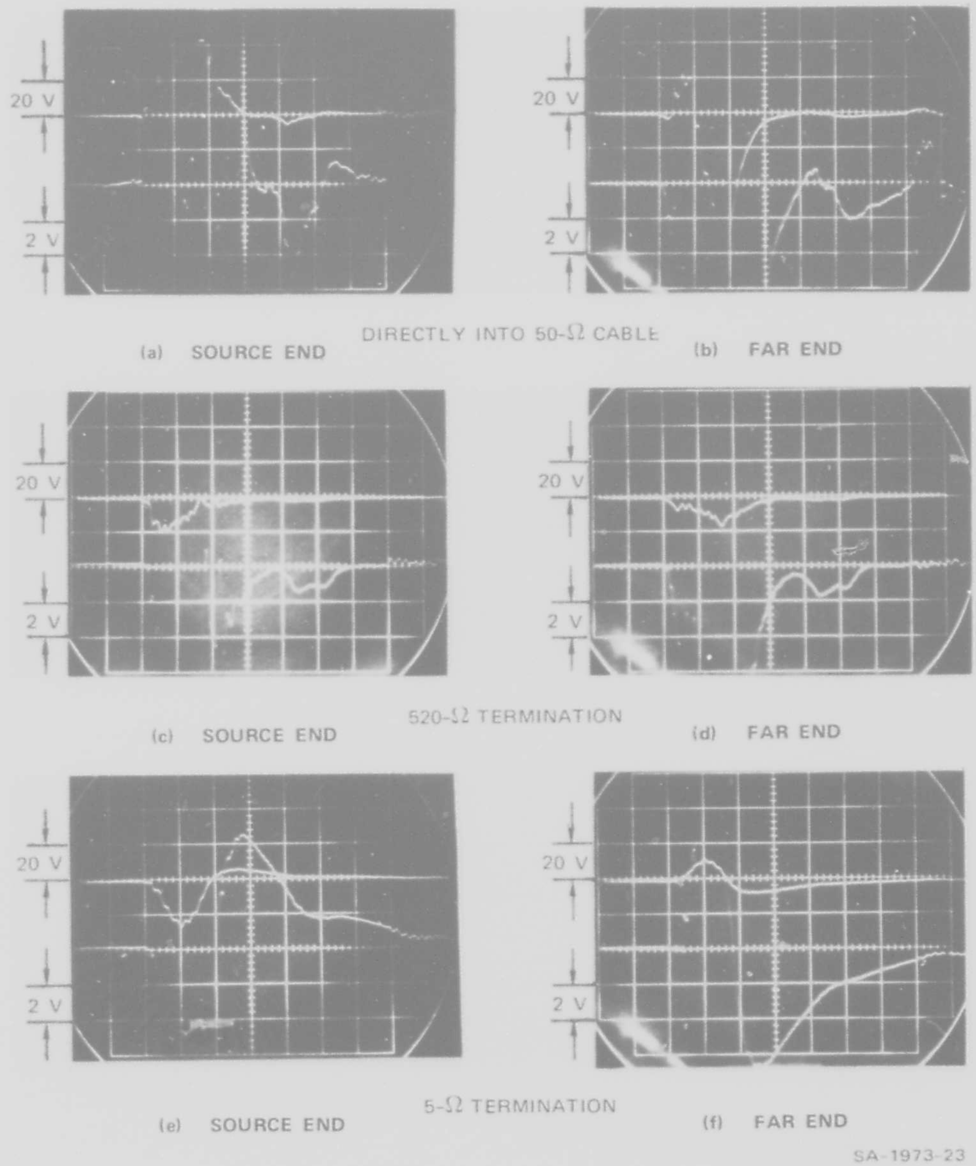


FIGURE C-3 LONGITUDINAL WIRE LINE, 21" LONG, 6" OVER GROUND PLANE